Symbol Period based Energy Detector

Shaik Nagulushareef

A Thesis Submitted to

Indian Institute of Technology Hyderabad

In Partial Fulfillment of the Requirements for

The Degree of Master of Technology

भारतीय प्रौद्योगिकी संस्थान हैदराबाद
Indian Institute of Technology Hyderabad

Department of Electrical Engineering

June 2016

Declaration

I declare that this written submission represents my ideas in my own words, and where ideas or words of others have been included, I have adequately cited and referenced the original sources. I also declare that I have adhered to all principles of academic honesty and integrity and have not misrepresented or fabricated or falsified any idea/data/fact/source in my submission. I understand that any violation of the above will be a cause for disciplinary action by the Institute and can also evoke penal action from the sources that have thus not been properly cited, or from whom proper permission has not been taken when needed.

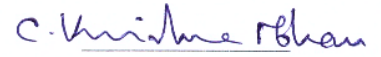SK. Nagulushareef

(Signature)

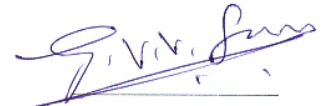SHAIK NAGULUSHAREEF

(Shaik Nagulushareef)

EE14MTECH11011

(Roll No.)

Approval Sheet

This Thesis entitled Symbol Period based Energy Detector by Shaik Nagulushareef is approved for the degree of Master of Technology from IIT Hyderabad

(Dr. C. Krishna Mohan) Examiner
Department of Computer Science and Engineering
IITH

(Dr. GVV Sharma) Examiner
Dept. of Electrical Engineering
IITH

(Prof. Mohammed Zafar Ali Khan) Adviser
Dept. of Electrical Engineering
IITH

Acknowledgements

I would like to thank almighty who bestowed good people and atmosphere around me. I am very grateful to my family for their trust on me to pursue my masters degree. My special thanks to my guide Prof.Mohammed Zafar Ali Khan who is always inspiration for me to excel in academics and research. Prof. Mohammed Zafar Ali Khan has given best advices and suggestions throughout my M.Tech at IIT Hyderabad. I am very thankful to the faculty of EE department at IITH without their teaching I can't be good at concepts in my subjects.

I owe special thanks to research students Sigabath Ali Khan, Narasimha Bhanavathu, Abdul Mateen, Amaralingam Madapu and Mohammed Fayazur Rahaman for their encouragement and suggestions in my thesis work. I am extremely grateful to Mohammed Abdullah Zubair for his tolerence and reflection of positive attitude. I am also thankful to all my classmates and labmates for their company in classrooms and labs. I am very thankful to many unmentioned friends who made my stay at IITH enjoyable.

Finally, I would like to thank TVWS team at IIT Hyderabad.

Dedication

To my parents, sister and brother

for their love, support and encouragement

Abstract

This thesis deals with signal detection which is very essential in wireless communications, RADAR and Cognitive radio. In particular, detection of digitally modulated signals is considered in this thesis. Due to presense of carrier in digital modulated signal, certain symmetries can be identified in the received signal. Assuming the knowledge of signal bandwidth, we propose a novel detector for digital modulated signals using identified symmetry properties. A very good amount of literature survey is given for existing detectors and followed by design and analysis of our proposed detector named Symbol PEriod based Energy Detector(SPEED). Extensive simulation results are given for BPSK and 16-QAM signals to corrobarate analysis of SPEED and are compared with Conventional energy detector, Improved energy detector and Cyclostationary detector. These results show that SPEED performs much better than other detectors.

We also analyze computational complexity of SPEED and compare with existing detectors. This analysis clearly depicts the reduction in computational complexity of SPEED. Computations are reduced by half when compare with Conventinal energy detector. Simulation results also show that performance degradation in SPEED is negligible due to the frequency mismatch at the receiver.

Contents

Chapter 1

Introduction

1.1 Introduction

Signal detection is considered as one of the most fundamental problem and as such has been well studied in RADAR, spectrum sensing for cognitive radio and in wireless communication systems. In general, signal detection performance is characterized by Receiver Operating Characteristics (RoC), which is a plot between probability of false alarm (P_F) and probability of detection (P_D). P_F is completely dictated by the noise considered in the signal detection problem. P_D depends on SNR of the received signal. In practical applications, we require a detector which achieves high P_D with low computational complexity as such the Conventional Energy Detector (CED) is a popular choice. Optimal detectors which maximize the P_D may not be practically feasable to implement as they often suffers from high computational complexity. Design and analysis of optimal detectors is often very cumbersome due to complexity of mathematics involved and results in loss of intuition. Hence, It is of our interest to design suboptimal detectors by using the knowledge available about the signal for its detection. Suboptimal detectors can give good performance as comapared with optimal detectors and involes very less computation when compare with optimal detectors.

When prior information about primary user signal is not available, the obvious choice of the detector is energy detector. Hence, it is very certain that in most of the cases energy detector is not optimal. When some information about primary signal (probability distribution) is available, we can design optimal detectors assuming noise signal is additive white gaussian noise (AWGN). When we have additional information such as waveform shape and period, we can further design better detector such as matched filter detector. Hence as the information about primary user signal

increases, probability of detection also increases.

1.2 Related work

CED compares the received signal energy against a threshold to detect the presence or absence of a signal and is the simplest[1]. The Matched Filter Detector (MFD) correlates the received signal with a copy of the transmitted signal and compares with a threshold. As such, it is also computationally simple but requires knowledge of the signal, which may not be practical at the detection stage as the receiver has not yet synchronized with the transmitter. Cyclostationary feature detectors extracts inherent symmetry in communication signals in terms of cyclic frequency which depends on the carrier frequency [2]. Cyclostationary detectors however have practical limitations due to cyclic frequency mismatch and computational complexity. Comprehensive surveys on spectrum sensing can be found in [1],[3]. Signal detection is being studied as problem of spectrum sensing in cognitive radio. Excellent treatment of conventional energy detector was considered in [4]. In [5], Chen proposed improved energy detector(IED) by replacing square operation in CED with power p for which probability of detection is maximized. Computationally efficient algorithms to analyse cyclostationary signls was given in [6]. Magnitude squared coherence(MSC) function of cyclostationary signals and detection is considered in [7]. Performance comparison of various spectrum sensing techniques is considered in [2].

1.3 Organization and Main contributions of the Thesis

A few signal detection techniques which are very popular because of their low complexity and noncoherent in nature are given in the following chapter with detailed description. They are conventional energy detector(CED), Improved energy detector(IED) and cyclostationary detector. Main contribution of this thesis is design and analysis of new detector for digital modulation signal detection and comaparing with other detectors. Proposed detector is also useful for Code Division Multiple Access (CDMA) and tone modulated signals as well. The following is summarizes the contrinutions of this thesis.

In this thesis, we propose Symbol PEriod based Energy Detector (SPEED) which is suitable for most digital modulated signals. SPEED exploits the symmetry in the received signal due to the symbol duration by appropriately choosing the intermediate frequency and the sampling rate. The test statistic for SPEED is obtained by suitably modifying the CED test statistic. We then

derive analytical expressions of P_F and P_D and verify the performance of the proposed detector with simulations for the case of BPSK and 16-QAM signals. We also give computational complexity of SPEED and compare with other detectors with favourable results.

This thesis is organized as follows. In chapter 2, we give good survey of existing detectors and their theoretical analysis. In chapter 3, we present the discrete signal model of a digital modulated signal for signal detection in a practical scenario. We then develops the symmetry properties inherent in a digital modulated signal and then present the SPEED that exploits the symmetry properties. We derive analytical expressions for P_F and P_D for the proposed SPEED. We compare the computational complexity of all the detectors. In chapter 4, we give present simulation results for BPSK and 16-QAM signals, followed by summary and discussions in chapter 5.

Chapter 2

Existing Detectors

2.1   Introduction

The signal detection can be considered as a binary hypothesis testing problem with multiple observations [8], such that

$$H_0 : y_i[n] = w[n]$$
$$H_1 : y_i[n] = x_i[n] + w[n] \tag{2.1}$$

where $0 \leq n \leq N_b - 1, 0 \leq i \leq N - 1$, $y_i[n]$ represents n^{th} sample in i^{th} received symbol, N is the number of symbol durations and $w[n]$ is Additive White Gaussian Noise (AWGN) with zero mean and variance σ^2.

We assume that the ensemble average energy of the message signal is unity, i.e.

$$E\{|x_i[n]|^2\} = E\{|m_i|^2\} = 1 \tag{2.2}$$

where $m_i = m_{ir} + jm_{iq}$.

In general, performance of the detector is characterized by Receiver Operating Characteristics(ROC). ROC is the plot between Probability of false alarm(P_F) and probability of detection(P_D). P_F and P_D can derived from probability density function(pdf) of teststatics for the binary hypothesis testing problem. P_F is derived from the pdf of teststatic using the case of null hypothesis. P_D

is derived from the pdf of teststatic when we have alternative hypothesis. Mathematically,

$$P_F Z = Pr(T(y/H_0) > \lambda), \tag{2.3}$$

$$= \int_\lambda^\infty f_{T(y/H_0)}(y) dy \tag{2.4}$$

$$= 1 - CDF\{T(y/H_0)\} \tag{2.5}$$

and

$$P_D = Pr(T(y/H_1) > \lambda), \tag{2.6}$$

$$= \int_\lambda^\infty f_{T(y/H_1)}(y) dy \tag{2.7}$$

$$= 1 - CDF\{T(y/H_1)\} \tag{2.8}$$

where $T(Y/H_0)$ is the teststatic for null hypothesis(H_0) and $T(Y/H_1)$ is the teststatic for alternative hypothesis(H_1). λ is the threshold which is critical to take decision. If calculated teststatic is greater than threshold, we consider it as presence of signal. If teststatic is less than threshold, it will be considered as noise.

In this chapter, we present the literature survey of practcle detectors used in wireless communications and cognitive radio. In the next section, detailed description of conventional energy detector is given followed by improved energy detector. Finally, we give cyclostationary of signal and detection. Further, we conclude the chapter by summarising the key points regarding existing detectors.

2.2 Conventional Energy Detector

The teststatic for the conventional energy detector (CED) is given by,

$$T(y) = \frac{1}{NN_b} \sum_{n=1}^{NN_b} \left(\frac{|y[n]|}{\sigma} \right)^2 \overset{H_0}{\underset{H_1}{\lessgtr}} \lambda \tag{2.9}$$

CED teststatic involves simply squaring and additional operations. Hence, it has very low computational complexity. CED is also a noncoherent detector which is often used when we have no knowledge about singal of our interest for detection. Due to this, Most of the times CED is the natural choice for signal detection of any kind of signal. Hence, In this thesis, we treat CED as

benchmark for all other detectors.

(2.9) is a sum of squares of guassian random variable which is written as chi-square disibution. In the case of H_0, each gaussian random variable in (2.9) has zero mean and unity variance. Hence, In H_0 case 2.9 follows central chi-square distribution with degrees of freedom (k) is given as NN_b. Degrees of freedom is the number of terms in the summation given in (2.9). In the case of H_1, each guassian random variable in (2.9) has unit variance and mean is governed by the signal under consideration. Hence, $T(Y/H_1)$ follows noncentral chi-square distribution with degrees of freedom is given as NN_b and non-central parameter is defined as follows:

$$\gamma = \sum_{i=1}^{NN_b} \mu_i^2 \tag{2.10}$$

where μ_i is the mean of the ith guassian random variable in (2.9).

The pdf of a central chi-square distribution is given by [9]

$$f(x;k) = \frac{1}{2^{\frac{k}{2}}\Gamma(\frac{k}{2})} x^{\frac{k}{2}-1} e^{\frac{-x}{2}}, \tag{2.11}$$

and the pdf of noncentral chi-square distribution is given by [9]

$$f(x;k,\lambda) = \frac{1}{2} e^{\frac{-(x+\lambda)}{2}} \left(\frac{x}{\lambda}\right)^{\frac{k}{4}-\frac{1}{2}} I_{\frac{k}{2}-1}\left(\sqrt{\lambda x}\right), \tag{2.12}$$

From the pdf expressions, we can derive P_F and P_D expressions for CED. The expression for P_F is given as,

$$P_F = 1 - F_{T(Y/H_0)}\left(\frac{k}{2}, \frac{\lambda}{2}\right) \tag{2.13}$$

From (2.13), threshold is given by

$$\lambda = 2F_{T(Y/H_0)}^{-1}\left(\frac{k}{2}, 1 - P_F\right) \tag{2.14}$$

6

Probability of detection(P_D) is given by

$$P_D = Q_{k/2}\left(\sqrt{\gamma}, \sqrt{\lambda}\right) \qquad (2.15)$$

Hence, ROC equation is given as,

$$P_D = Q_{k/2}\left(\sqrt{\gamma}, \sqrt{2F_{T(Y/H_0)}^{-1}\left(\frac{k}{2}, 1 - P_F\right)}\right), \qquad (2.16)$$

where $F_{T(Y/H_0)}(a, x)$ is given by incomplete gamma function which is CDF of central chi-square distribution [9] and it is defined as follows:

$$F_{T(Y/H_0)}(a, x) = \frac{1}{\Gamma(a)}\int_0^x e^{-t}t^{a-1}dt \qquad (2.17)$$

$Q_M(a, b)$ is Marcum-Q-function which is given by [9]

$$Q_M(a, b) = \int_b^\infty x\left(\frac{x}{a}\right)^{M-1}\exp\left(-\frac{x^2 + a^2}{2}\right)I_{M-1}(ax)dx \qquad (2.18)$$

with modified bessel function I_{M-1} of order $M - 1$.

2.3   Improved Energy Detector

Improved Energy detector(IED) is slight modification of CED. The exponent 2 operation in CED is replaced by p where p can be varied to maximize the P_D. The teststatic for IED is given as follows:

$$T'(y) = \frac{1}{NN_b}\sum_{n=1}^{NN_b}\left(\frac{|y[n]|}{\sigma}\right)^p \underset{H_1}{\overset{H_0}{\lessgtr}} \lambda' \qquad (2.19)$$

Here, probability distributions of (2.19) varies with p. Probability distributions of teststatics are approximately using noncentral chi-square distribution with suitable parameters. Further analysis of IED is given in [5].

2.4 Cyclostationary detector

Digitally modulated signals are cyclostationary signal due to presense of carrier, repeated waveforms and symbols. Cyclostationary features of the signal can be extracted by estimaing spectral density function or Magnitude squared coherence function for the given samples of the signal.

2.4.1 Spectral correlation density function

Spectral correlation density(SCD) is extension of power spectrum. SCD is evaluated by shifting the singal by cylclic frequency(α). Since AWGN is a stationary process, it doesn't exhibit spectrum at non zero cyclic frequency(α). Digital modulated signals are cyclostationary by nature due to sinusoidal carrier and repetitive codes. Hence by evaluating spectral correlation density (SCD) of received signal at appropriately chosen $\alpha \neq 0$, the signal and AWGN can be separated.

It is given as follows:

$$
\begin{aligned}
H0 &: \quad S_y^\alpha(f) = S_w^\alpha(f) \\
H1 &: \quad S_y^\alpha(f) = S_x^\alpha(f) + S_w^\alpha(f)
\end{aligned}
\tag{2.20}
$$

where $S_y^\alpha(f)$ is the spectral correlation density and is given as follows:

$$
S_y^\alpha(f) = \int\limits_{-\infty}^{\infty} R_y^\alpha(\tau) \exp^{-i2\pi f\tau} dt
\tag{2.21}
$$

$R_y^\alpha(\tau)$ is cyclic autocorrelation and is given by

$$
R_y^\alpha(\tau) = \lim_{T->\infty} \int\limits_{-\infty}^{\infty} x(t+\tau/2)x^*(t-\tau/2) \exp^{-i2\pi\alpha t} dt
\tag{2.22}
$$

Cyclic spectral analysis alogorithm fall into two categories. one is time smoothing algrithms and other is frequency smoothing algorithms. Time smoothing algorithms are considered as computationally efficient than frequency smmothing algorithms. There are popular algorithms to estimate SCD of a signal. They are FFT accumulation method (FAM) and strip spectral correlation algogorithm(SSCA). Since FAM is more computationally efficient than SSCA, we conder estimation

SCD using FAM.

FFT Accumulation method for estimating the SCD

FFT Accumulation Method(FAM) method incorporates the idea of time smoothing using FFT (Fast Fourier Transform) and which can be implemented digitally using samples of the signal. For given K samples of the signal, signal is divided into blocks of length N' such that succesive blocks have overlap of 75 %. Then , FFT of each block performed followed by frequency shifting $\frac{\alpha}{2}$. The value of N' depends on frequency resolution required and chosen as $N' = \frac{f_s}{\delta f}$. Later, time smoothing is done using P point FFT and the value of P is chosen as $P = \frac{f_s}{K\delta\alpha}$. Generally, the value of K is chosen as $\frac{N'}{4}$. Here, f_s denotes sampling frequency and δf and $\delta\alpha$ denotes frequency resolution and cyclic frequency resolution respectively. Block diagram of the FAM is given below.
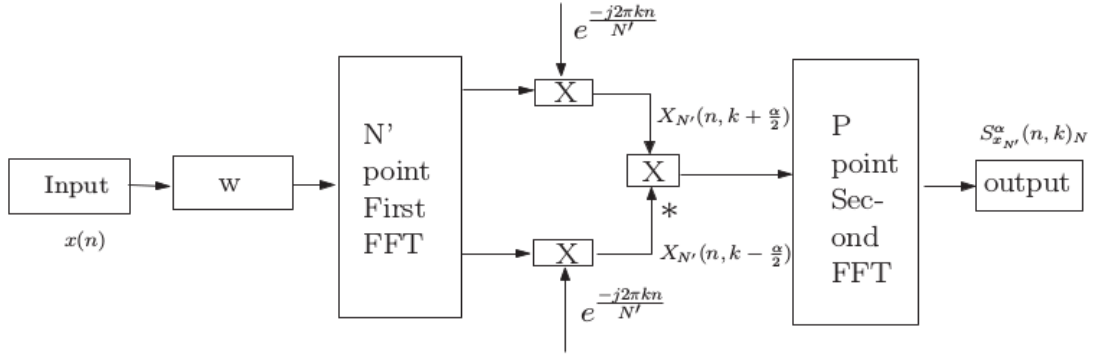

Figure 2.1: FAM block diagram[2]

2.4.2 Magnitude squared coherence function

The spectral autocoherence of a signal $x(t)$ at cyclic frequency(α) and spectrum frequency(f) is defined as [2]

$$C_x^\alpha = \frac{S_x^\alpha(f)}{[S_x^0(f - \frac{\alpha}{2})S_x^0(f - \frac{\alpha}{2})]^{\frac{1}{2}}} \tag{2.23}$$

(2.23) can also be written as follows:

$$C_x^\alpha = \frac{S_{uv}(f)}{\sqrt{S_u(f)S_v(f)}} = \gamma_{uv}(f) \tag{2.24}$$

where $S_u(f)$ and $S_v(f)$ are power spectral densities of $u(t)$ and $v(t)$, and $S_{uv}(f)$ is cross spectral density. Here, $u(t) = x(t)e^{-i\pi\alpha t}$ and $v(t) = x(t)e^{i\pi\alpha t}$ are frequency shifted versions of x(t). The magnitude squared coherence is defined as $|\gamma_{uv}(f)|^2$. In practice, MSC is estimated as follows:

Let $u[n]$ and $v[n]$ denote N-length complex sequences which are segmented with 75% overlap, segments $u_l[n]$ and $v_l[n]$, l=1,2..L, each of lengh M. Let $U_l(k) = F(u_l[n])$ and $V_l(k) = F(v_l[n])$, where $F()$ denotes FFT opetation. From these, spectral densities are estimated as follows:

MSC Estimation

$$\hat{S}_u(k) = \sum_{l=1}^{L} |U_l(k)|^2$$
$$\hat{S}_v(k) = \sum_{l=1}^{L} |V_l(k)|^2 \tag{2.25}$$

and

$$\hat{S}_{uv}(k) = \sum_{l=1}^{L} |U_l(k)V_l^*(k)|^2 \tag{2.26}$$

From this, MSC is estimated as follows

$$|\gamma_{uv}(f)^2| = \frac{|\hat{S}_{uv}(f)|^2}{\hat{S}_u(f)\hat{S}_v(f)} \tag{2.27}$$

2.5 Chapter Summary

In this chapter, we give detailed literature about CED, IED and CSD. Conventionally, energy detector is popular choice for unknown signals. When exponent 2 in the CED is replaced with p, we get improved energy detector. IED gives better performance than CED at low SNR values. Analytically, IED is very difficult to analyse but using simulations we can show slight gain in the performance over CED. Cylcostationary features in the digital modulated signals can be used to detect signal. Magnitude squared coherence detector is better than Spectral correlation density detector [2]. Magnitude

squared coherence(MSC) detector performace depends on segment size, overlap among segments and correlation between samples. Hence, Eventhough MSC detector is noncoherent, we need to take care of different parameters which can affect the performace of detector drastically.

Chapter 3

The SPEED

3.1   Introduction

In this chapter, practical signal detection model has been considered. Practicle signals are transmitted at higher frequencies which are downconverted to some intermediate frequency. This signal is sampled and applied to the detector which is designed based on symmetry present in the signals. Due to presence of carrier in the digital modulation signals, we can observe certain kind of symmetry in their waveform. Using the symmetries in the time domain of the signal, we design Symbol PEriod based Energy Detector(SPEED). SPEED is also an energy detector but its parameters are different from conventional energy detector. In SPEED, we align the samples and multiply with the complex exponential to coherently add the signal samples. This coherent addition will boost the SNR of the signal which results in better detection probability than other detectors. Since SPEED uses only additions and multiplications, its comupational complecity is comparable to that of CED. In some cases, computational complexity of SPEED is the least when it is compared with other detectors. This is acheived by properly choosing down conversion frequency and sampling frequency which is often choice of designer.

3.2 Practical Signal Detction Model

In general, a digital modulated signal is given by [10],

$$x_i(t) = Re\{(m_{ir} + jm_{iq})g(t)e^{j2\pi f_c t}\}$$
$$= m_{ir}g(t)cos(2\pi f_c t) - m_{iq}g(t)sin(2\pi f_c t),$$

(3.1)

where $0 \leq t \leq T_b$, T_b denotes the symbol duration and $i = 0, 1, \cdots$ is the symbol index. We assume $g(t)$ is a rectangular waveform with bandwidth $W = 1/T_b$. At the receiver, the signal is down converted to an intermediate frequency f_0 and then passed through a low pass filter. The corresponding in-phase component is given by

$$x_{ir}(t) = m_{ir}\cos(2\pi f_0 t + \theta) - m_{iq}\sin(2\pi f_0 t + \theta),$$

(3.2)

where θ is the phase shift. The quadrature component is similarly given by

$$x_{iq}(t) = m_{ir}\sin(2\pi f_0 t + \theta) + m_{iq}\cos(2\pi f_0 t + \theta).$$

(3.3)

Note that as we intend to derive the symmetry in the received signal, the noise component is neglected initially. The signals $x_{ir}(t)$ and $x_{iq}(t)$ are then sampled at $t = nT_s$ where $T_s = \frac{T_b}{N_b}$, where N_b is an integer (the period of the discrete time signal). Assuming $T_s f_0 = \frac{1}{N_s}$ where $KN_s = N_b, K \in \{1, 2, \cdots\}$, the corresponding discrete time signal is given by

$$x_i[n] = x_{ir}[n] + jx_{iq}[n], \quad n = 0, 1, \cdots, N_b - 1, \quad i = 0, \cdots, N - 1,$$

(3.4)

where

$$x_{ir}[n] = m_{ir}cos\left(\frac{2\pi n}{N_s} + \theta\right) - m_{iq}sin\left(\frac{2\pi n}{N_s} + \theta\right),$$
$$x_{iq}[n] = m_{ir}sin\left(\frac{2\pi n}{N_s} + \theta\right) + m_{iq}cos\left(\frac{2\pi n}{N_s} + \theta\right),$$

(3.5)

which can be compactly represented as

$$x_i[n] = (m_{ir} + jm_{iq})e^{j\left(\frac{2\pi n}{N_s} + \theta\right)},$$

(3.6)

13

where m_{ir} and m_{iq} are the in-phase and quadrature components of the message symbol respectively and N_b is the number of samples per symbol duration and is assumed to be an integer.

Remark 1 *Note that in the signal model presented in this paper there are two important assumptions,*

1. *first the intermediate frequency is assumed to be an integer multiple of the signal bandwidth and*

2. *second the sampling frequency is an integer multiple of the signal bandwidth.*

These assumptions are essential for extracting the carrier symmetry as will be apparent in later sections. However these assumptions are not restrictive as both the intermediate frequency and sampling frequency are receiver design parameters that are not fixed by any standard and the designer has the flexibility to choose them appropriately.

Remark 2 *Note that this model can be used to represent various other signals which are enumerated below:*

1. *using $m_{ir} + jm_{iq} = 1, \forall i$, the signal model of (3.6) can be used to represent the received signal when a **tone** is transmitted.*

2. *assuming $m_{ir} + jm_{iq}$ to be the product of the message symbol and chipping sequence, (3.6) can be used to represent a **CDMA** signal with T_b representing the chip duration.*

3.3   Symmetry properties in digital modulation signals

We define

Definition 1 (Half wave Symmetry) *A given signal $x[n]$, with period N_b, is said to exhibit half wave symmetry if*

$$x[n] = \mp x\left[n + \frac{N_b}{2}\right], \qquad 0 \leq n \leq \frac{N_b}{2} - 1. \tag{3.7}$$

Definition 2 (Rotational Symmetry) *A given signal $x[n]$, with period N_b, is said to exhibit rotational symmetry if*

$$x[n] = x[n-k]e^{\frac{j2\pi k}{N_s}}, \qquad 0 \leq k \leq n \leq N_b - 1. \tag{3.8}$$

We now show that any digital modulated signal exhibits rotational symmetry.

Propositon 1 *A digital modulated signal exhibits rotational symmetry.*

Proof

Consider the discrete signal $x_i[n-k]e^{\frac{j2\pi k}{N_s}}$ where $x_i[n]$ is as defined in (3.6). Substituting from (3.6) and simplifying, we have

$$
\begin{aligned}
x_i[n-k]e^{\frac{j2\pi k}{N_s}} &= m_i e^{j\left(\frac{2\pi(n-k)}{N_s}+\theta\right)} e^{\frac{j2\pi k}{N_s}} \\
&= m_i e^{j\left(\frac{2\pi n}{N_s}+\theta\right)} \\
&= x[n]
\end{aligned}
\tag{3.9}
$$

completing the proof.

When N_b is even the digital modulated signal exhibits additional symmetry. We have

Propositon 2 *A digital modulated signal exhibits half wave symmetry when the symbol duration, N_b, is a even integer.*

Proof

Using the signal model given in (3.6), we have

$$
\begin{aligned}
x_i\left[n+\frac{N_b}{2}\right] &= m_i \exp\left\{j\left(\frac{2\pi\left(n+\frac{N_b}{2}\right)}{N_s}+\theta\right)\right\} \\
&= m_i e^{\frac{j2\pi n}{N_s}} e^{j\pi K} \\
&= (-1)^K m_i e^{\frac{j2\pi n}{N_s}} \\
&= \mp x[n].
\end{aligned}
\tag{3.10}
$$

3.4 SPEED testatics

We now present the statistic of an energy detector that takes utilizes the symmetry, presented in section 3.3, in a digital modulated signal.

N_b Odd

Using Proposition 1, when N_b is odd, $x_i[n]$ signal exhibits rotational symmetry. Hence, we can align the samples within a symbol duration as $\sum_{n=0}^{N_b-1} x_i[n]e^{\frac{-j2\pi n}{N_s}}$. Applying the same logic to the received

samples $y_i[n]$ and then taking the energy of the aligned samples within a symbol to give the test statistic

$$T(Y) = \frac{2}{N_b\sigma^2} \sum_{i=1}^{N} \left| \sum_{n=0}^{N_b-1} y_i[n] e^{\frac{-j2\pi n}{N_s}} \right|^2. \tag{3.11}$$

N_b even

When N_b is even, $x_i[n]$ exhibits both half wave and rotational symmetry. Following the odd case, we can write test statistic for even N_b as

$$T(Y) = \frac{2}{N_b\sigma^2} \sum_{i=1}^{N} \left| \sum_{n=0}^{\frac{N_b}{2}-1} \left(y_i[n] \mp y_i \left[n + \frac{N_b}{2} \right] \right) e^{\frac{-j2\pi n}{N_s}} \right|^2. \tag{3.12}$$

Remark 3 *Propositions 1,2 present symmetry in a digital modulated signal for all $K \in \{1, 2, \cdots\}$ and in-particular for $K = 1$. When $K > 1$, a digital modulated signal offers more symmetry due to multiple cycles of the carrier. The test statistics in (3.11) and (3.12) can be further sharpened to incorporate the symmetry offered by the multiple carries. The corresponding test statistic, for odd N_b, is given by*

$$T(Y) = \frac{2}{N_b\sigma^2} \sum_{i=1}^{N} \left| \sum_{n=0}^{N_s-1} \left(\sum_{l=0}^{K-1} y_i[n + l * N_s] \right) e^{\frac{-j2\pi n}{N_s}} \right|^2, \tag{3.13}$$

and for even N_b is given by (3.14).

$$T(Y) = \frac{2}{N_b\sigma^2} \sum_{i=1}^{N} \left| \sum_{n=0}^{\frac{N_s}{2}-1} \left\{ \sum_{l=0}^{K-1} \left(y_i[n + lN_s] \mp y_i \left[n + lN_s + \frac{N_s}{2} \right] \right) \right\} e^{\frac{-j2\pi n}{N_s}} \right|^2. \tag{3.14}$$

In what follows, we assume $K = 1$ for simplicity.

3.5 SPEED Analysis

We now derive the probability of false alarm and probability of detection for the SPEED whose test statistics are give by (3.11) and (3.12) corresponding to whether N_b is odd or even. We can observe from the test statistics that SPEED is also an energy detector. Hence, the probability distribution functions (pdf) of the test statistic of the SPEED also follows central and noncentral

chi-square distributions (as in the case of CED [4]) for the hypothesis H_0 and H_1 respectively; but with different parameters. In Subsection 3.5.1, we derive the parameters for the probability distributions of the test statistics given in (3.11) and (3.12)and then present the expressions for P_F and P_D in Subsection 3.5.2.

3.5.1   Parameters of the Probability distributions

N_b **even**

For the hypothesis H_1, $T(Y)$ in (3.12) follows noncentral chi-square distribution [8] with noncentrality parameter, λ, given by

$$\lambda = \frac{2N_b}{\sigma^2} \sum_{i=1}^{N} |m_i|^2 \tag{3.15}$$

and degrees of freedom, $k = 2N$. Using (2.2), ensemble average value of noncentrality parameter can be derived as

$$E[\lambda] = \frac{2NN_b}{\sigma^2}. \tag{3.16}$$

For the hypothesis H_0, $T(Y)$ in (3.12) follows central chi-square distribution with $k = 2N$.

N_b **odd**

Derivation of the parameters for N_b odd is similar to the case when N_b is even; for H_1, (3.11) follows noncentral chi-square distribution with noncentrality parameter given by (3.15), average value of noncentrality parameter given by (3.16) and the degrees of freedom (k) is given by $k = 2N$. For H_0 case, (3.11) follows central chi-square distribution $k = 2N$.

The degrees of freedom (k) and noncentrality parameter (λ) for the SPEED is summarized and compared with the CED in Table 3.1.

Table 3.1: Parameters of SPEED and CED

Parameters	SPEED	CED
k	$2N$	$2NN_b$
$E\left[\lambda\right]$	$\frac{2NN_b}{\sigma^2}$	$\frac{2NN_b}{\sigma^2}$

The pdf of a central chi-square distribution is given by [9]

$$f(x;k) = \frac{1}{2^{\frac{k}{2}}\Gamma(\frac{k}{2})} x^{\frac{k}{2}-1} e^{\frac{-x}{2}}, \tag{3.17}$$

and the pdf of noncentral chi-square distribution is given by [9]

$$f(x;k,\lambda) = \frac{1}{2} e^{\frac{-(x+\lambda)}{2}} \left(\frac{x}{\lambda}\right)^{\frac{k}{4}-\frac{1}{2}} I_{\frac{k}{2}-1}\left(\sqrt{\lambda x}\right), \tag{3.18}$$

where $I_v(y)$ is the modified bessel function of first kind.

3.5.2 P_F and P_D expressions

Following [4], the Probability of false alarm is given as

$$P_F = 1 - F(\tau;N) \tag{3.19}$$

where

$$F(\tau;N) = \frac{\gamma\left(N,\frac{\tau}{2}\right)}{\Gamma\left(N\right)}. \tag{3.20}$$

From (3.19), the threshold can be obtained as

$$\tau = 2F^{-1}\left(N, 1 - P_F\right). \tag{3.21}$$

The probability of detection is given as

$$P_D = Q_N \left(\frac{\sqrt{2NN_b}}{\sigma}, \sqrt{\tau} \right). \tag{3.22}$$

Hence, the RoC is characterized by

$$P_D = Q_N \left(\frac{\sqrt{2NN_b}}{\sigma}, \sqrt{2F^{-1}\left(N, 1 - P_F\right)} \right), \tag{3.23}$$

where F is the cumulative density function (cdf) of the central chi-square distribution, $\gamma(.,.)$ is the lower incomplete Gamma function, Γ is the Gamma function and Q_N is the Marcum Q-function [9].

3.6 Comparison of computational complexity

The number of computations required to compute a test statistic decides the practical feasibility of the detector and sensing duration required for a particular detection technique. Hence, it is of interest for us to find the computations required for CED, IED, SPEED and the MSC detector.

The computation require for the CED is calculated using test statistic given in [5]. It requires $2(NN_b - 1)$ real additions and $4(NN_b + 1) + 1$ real multiplications. Similarly, computation for IED is given using test statistic as given in [5]. It requires $2(NN_b - 1)$ real additions and $4p(NN_b + 1) + 2$ real multiplications, where p is the power operation replacing the exponent 2 in CED.

The computations required for SPEED can be calculated using (3.12) and (3.11). When N_b is even, SPEED requires $2(N - 1)(N_b - 1)$ additions and $2N_b(N + 1) - 1$ multiplications. When N_b is odd, it requires $2NN_b - 1$ additions and $2N_b(2N + 1) - 1$ multiplications.

As an example of a cyclostationary detector, we consider the Magnitude Squared Coherence (MSC) detector [2]. Note that the MSC has better computational complexity among known cyclostationary detectors; which is calculated as given below:

$Step$ 1: For frequency shifting, we need $8NN_b - 4$ real multiplications and $2NN_b - 2$ additions.

Table 3.2: Comparison of computational complexity for K=1

	Real Additions	Real Multiplications	Total Real Operations (Approx.)
CED	$2(NN_b - 1)$	$4(NN_b + 1)+1$	$6NN_b + 3$
IED	$2(NN_b - 1)$	$4p(NN_b + 1) + 2$	$NN_b(2 + 4p) + 4p$
SPEED (Even)	$2NN_b - 2N - 2N_b + 2$	$2NN_b + 2N_b - 1$	$4NN_b - 2N + 1$
SPEED (Odd)	$2NN_b - 1$	$4NN_b + 2N_b - 1$	$6NN_b + 2N_b - 3$
MSC	$26NN_b - 19M - 3$	$40NN_b - 20M - 4$	$32NN_b log_2 M + 18NN_b - 3M - 24M log_2 M - 7$

$Step\ 2$: Total number of segments of length M is $\frac{4NN_b}{M} - 3$. Assuming split radix FFT, as it requires the least number of computations [11] of $4M \log_2 M - 6M + 8$ additions and multiplications; the number of real multiplications and additions required for FFT of all segments for two frequency shifted signals is $2(\frac{4NN_b}{M} - 3)(4M \log_2 M - 6M + 8)$
$\approx 32NN_b \log_2 M - 48NN_b + 36M - 24M \log_2 M$.

$Step3$: To estimate spectral densities, we require $32NN_b - 24M$ real multiplications and $24NN_b - 21M$ real additions

$Step\ 4$: To estimate spectral correlation, we need $4M$ real multiplications and $2M - 1$ real additions. Hence the total computations required for MSC is $32NN_b log_2 M + 18M - 21NN_b - 24M log_2 M - 1$.

Table 3.2 summarizes the number of additions/subtractions, multiplications and divisions. Typically, p for IED is greater than 2. Observe that the computational complexity of the SPEED when the discrete period N_b is even is almost half of the CED. When the discrete period is odd then the complexity is almost same as that of CED. Also note that the computational complexity of SPEED is significantly smaller than IED and MSC.

Example 1 *Given the parameters* $N = 10, N_b = 10, K = 1$, $p = 3$ *and* $M = 16$, *Computations require for CED, IED, SPEED (Even), SPEED (Odd) and MSC are 603, 1412, 381, 617 and 13009 respectively.*

Remark 4 *Note that when* $K > 1$ *then the complexity of SPEED reduces by a factor of* K *as* $K - 1$ *multiplications are not required in each symbol period. Further when* $N_s = 2, 4$ *then the complexity of SPEED further reduces by a factor of two or four respectively. This is because the multiplications of the term* $e^{\frac{j2\pi n}{N_s}}$ *becomes trivial. As such significant reduction in complexity of SPEED can be obtained by proper design of* K, N_b, N_s *which in turn depend on choice of the intermediate frequency,* f_o, *and the sampling frequency,* f_s.

Table 3.3: Comparison of computational complexity for $K > 1$

	Real Additions	Real Multiplications	Total Real Operations (Apprx.)
CED	$2(NN_b - 1)$	$4(NN_b + 1)+1$	$6NN_b + 3$
IED	$2(NN_b - 1)$	$4p(NN_b + 1) + 2$	$NN_b(2 + 4p) + 4p$
SPPED (Even)	$2NN_b + 2N - NN_s + N_s - 4$	$2NN_s + 4N$	$2NN_b + 6N + NN_s + N_s - 4$
SPEED (Odd)	$2NN_b + 2N - 2NN_s + 2N_s - 4$	$4N(N_s + 1)$	$2NN_b + 6N + 2NN_s + 2N_s - 4$
MSC	$26NN_b - 19M - 3$	$40NN_b - 20M - 4$	$32NN_b log_2 M + 18NN_b - 3M - 24M log_2 M - 7$

For $K > 1$ also computational analysis is carrie out which is given in table 3.3. From the given table, we can observe the drastic reduction in the computational complexity of SPEED detector.

$$SPEED(even) < SPEED(odd) < CED < IED < MSC$$

Example 2 *Given the parameters* $N = 50, N_b = 24$, $N_s = 6$, $p = 3$ *and* $M = 16$, *Computations require for CED, IED, SPEED (Even), SPEED (Odd) and MSC are 7203, 16812, 3002, 3308 and 173609 respectively.*

Chapter 4

Results and Discussion

4.1 Simulation Results for K=1

In this section we present simulation results that corroborate the theoretical analysis for BPSK and 16-QAM modulations for various values of N_b, N. The intermediate frequency is set to $f_0 = 512$ KHz for all simulations except for frequency mismatch where we assume $f_c = 1MHz$, $f_0 = 300KHz$. Sampling frequency is taken as $fs = N_b f_0$. We use the results presented in [5], to simulate the performance of CED and IED. In IED, we use p values ranging from 1 to 10 with an interval of 0.1. For each P_F value, we choose a p value that maximizes the value of P_D. The MSC detector simulations follow [2] with length of each segment (M) of the signal equal to 64. SPEED is simulated by using (3.12) for the case of N_b even and (3.11) for the case of N_b odd. We use (3.23), to give theoretical plots of SPEED.

4.1.1 ROC Simulations

Figure 4.1 gives the simulation and theoretical results of RoC for SPEED and CED for 16-QAM modulated signals with $N = 10$ and $N_b = 8$ at SNR = -20 dB. From this plot, we can observe the exact match between theoretical and simulation results of CED and SPEED. Also this plot highlights the improved performance of SPEED as compared to the CED. We also observed that the SPEED has a SNR gain of approximately 3 dB as compared to CED (ie the RoC of the CED for SNR=-17dB matches the SPEED RoC for -20dB).
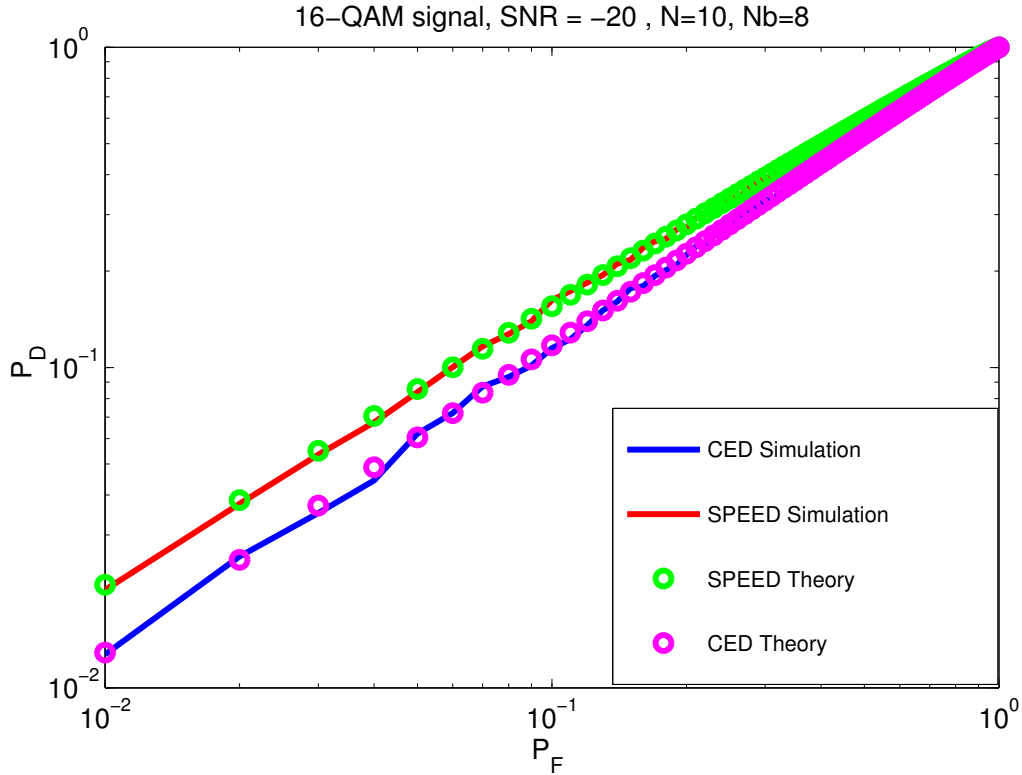
Figure 4.1: RoC for 16-QAM, $N = 10$, $N_b = 8$ at SNR=-20 dB.

Figure 4.2 gives the RoC plots of CED, IED, MSC detector and SPEED in the case of BPSK modulated signals with $N = 100, N_b = 8$ at SNR = -20 and -10 dB. Note that the SPEED significantly outperforms all other detectors. Since SPEED has different test statistics for even and odd, the RoC plots of all detectors in the case of BPSK modulated signals with $N = 100$, $N_b = 7$ at SNR = -20 and -10 dB in Fig. 4.3 with similar conclusions.

Similarly, the RoC of all the detectors are given for the case of 16-QAM signals with $N = 100$, $N_b=8$ at SNR = -20 and -10 dB in Fig. 4.4 and with $N_b = 7$ in Fig. 4.5 for 16-QAM modulated signals. From these plots, we can observe that the conclusions obtained from plots of BPSK modulated signals also hold for 16-QAM signals.
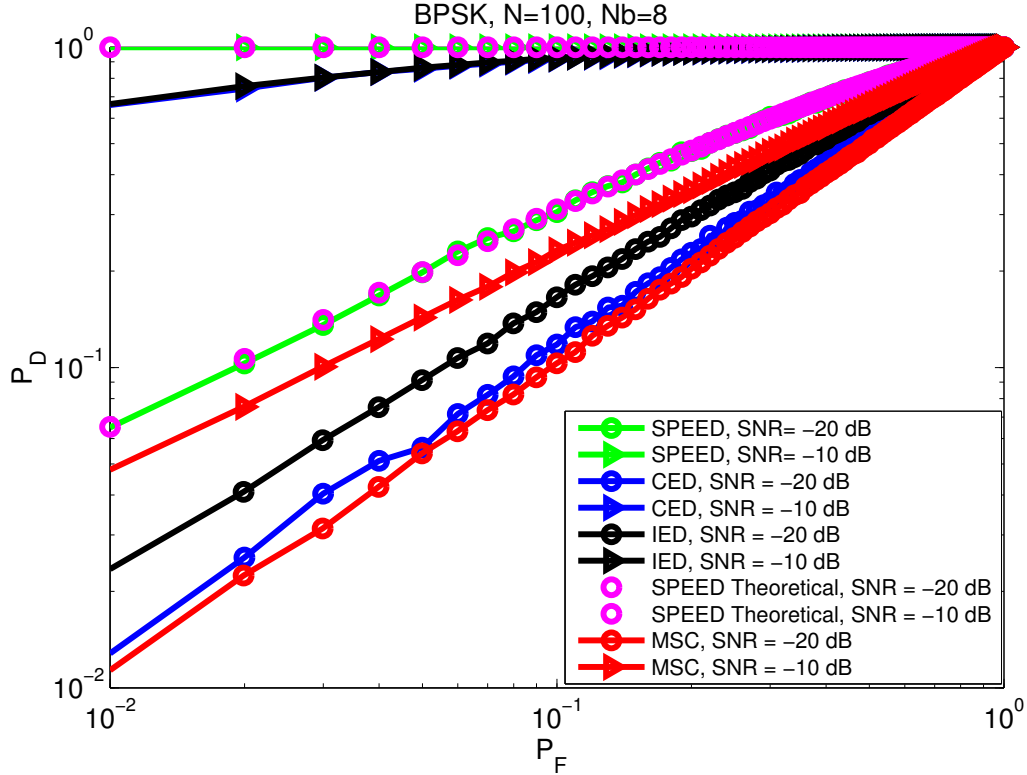
Figure 4.2: RoC for BPSK, $N = 100$, N_b=8.

We next show the performance improvement of SPEED as N_b increases. Figure 4.6 gives the RoC plots of SPEED and CED with $N = 100$, $N_b = 1, 2, 3, 4, 5, 6$ at SNR = -20 dB. Observe that at $N_b = 1$, SPEED is exactly same as CED. Also note that the SPEED starts to outperforms the CED from $N_b = 2$ and the performs improves as N_b increases.

In practical situations, there is always a frequency mismatch at the receiver. Hence, we simulate the RoC of the SPEED for BPSK modulated signals with frequency mismatch of 1, 100 and 10000 parts per million (ppm) in Fig. 4.7. Observe that the SPEED is as robust as CED for frequency mismatch.
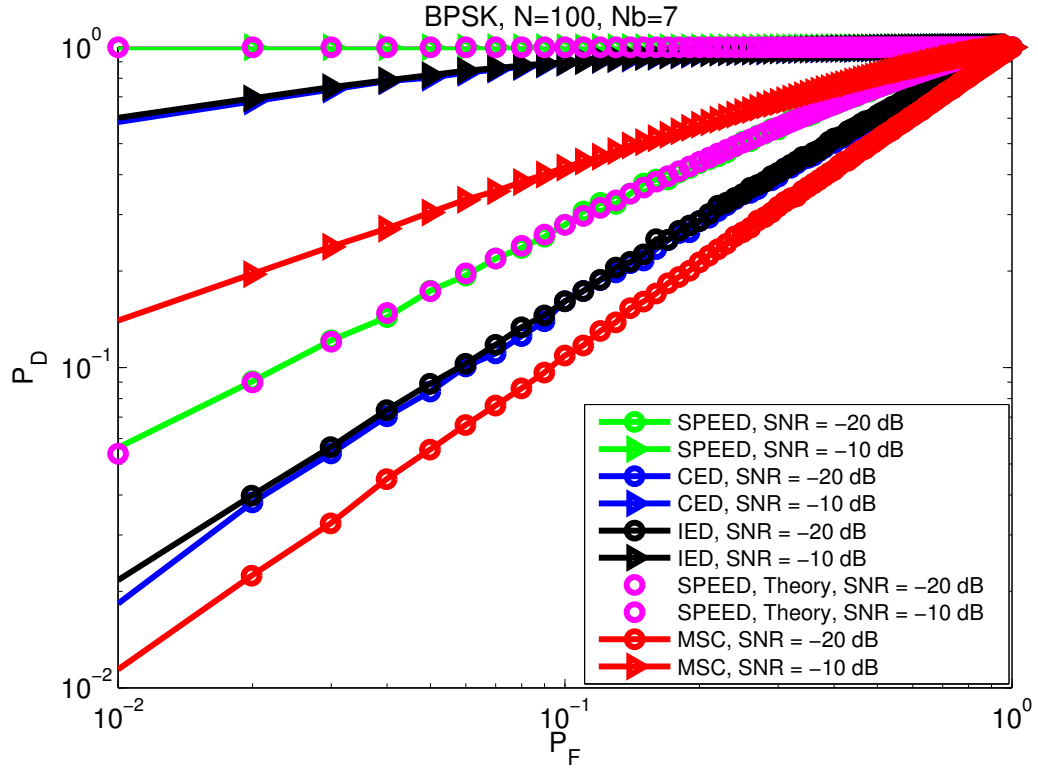
Figure 4.3: RoC for BPSK, $N = 100$, $N_b = 7$.
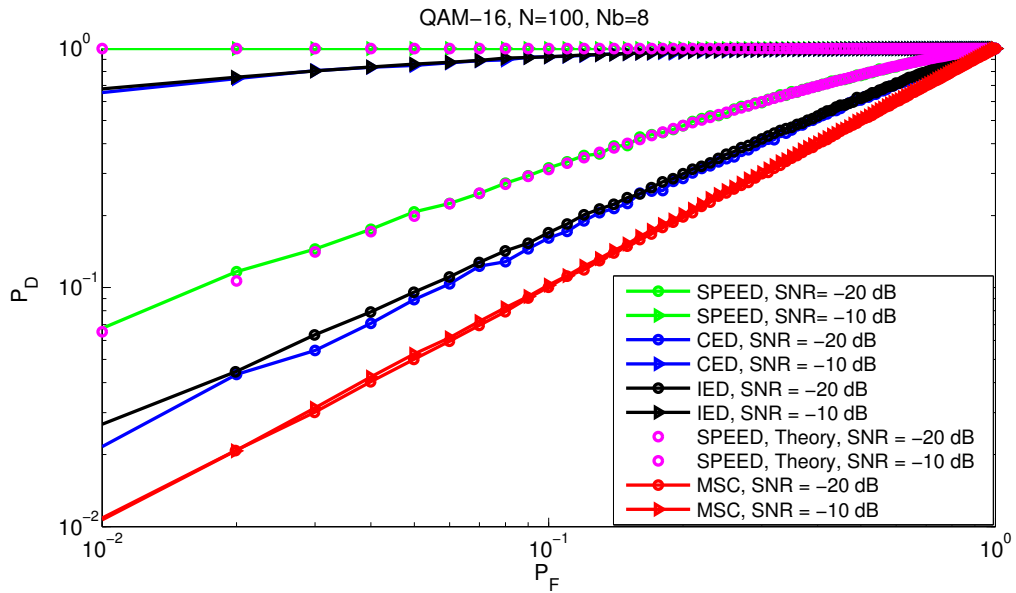
Figure 4.4: RoC for 16-QAM, $N = 100$, $N_b = 8$.
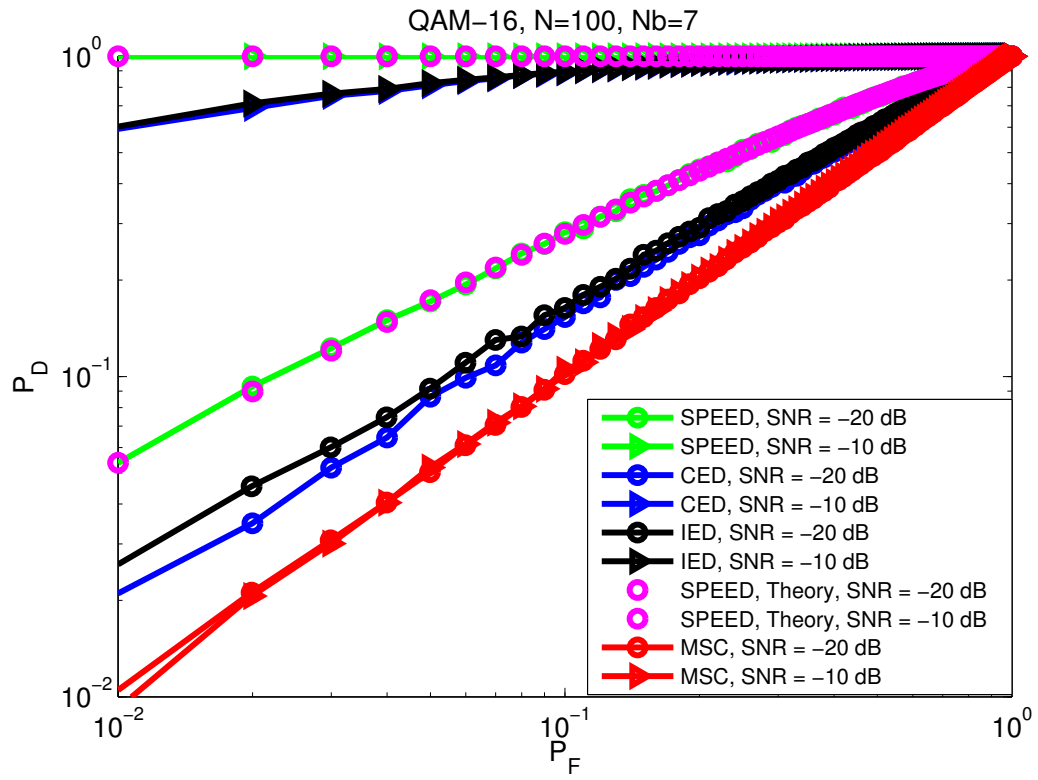
Figure 4.5: RoC for 16-QAM, $N = 100$, $N_b = 7$.
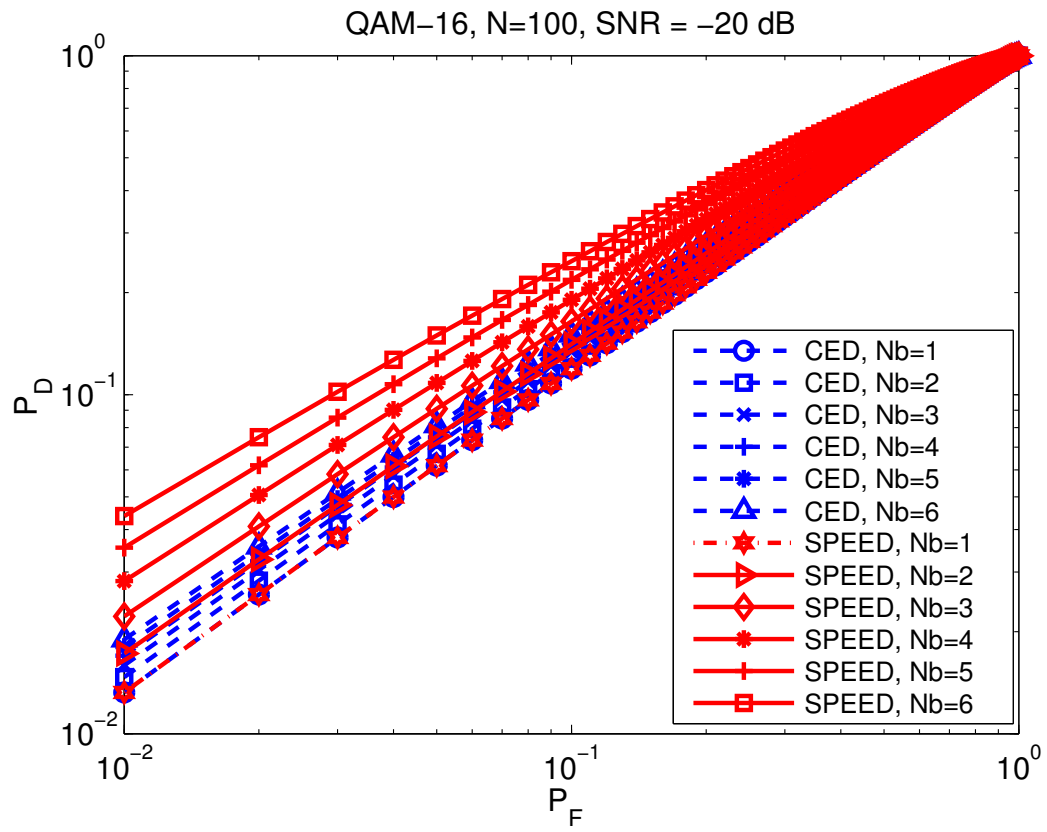
Figure 4.6: P_F vs. P_D for 16-QAM, $N = 100$ with varying N_b.
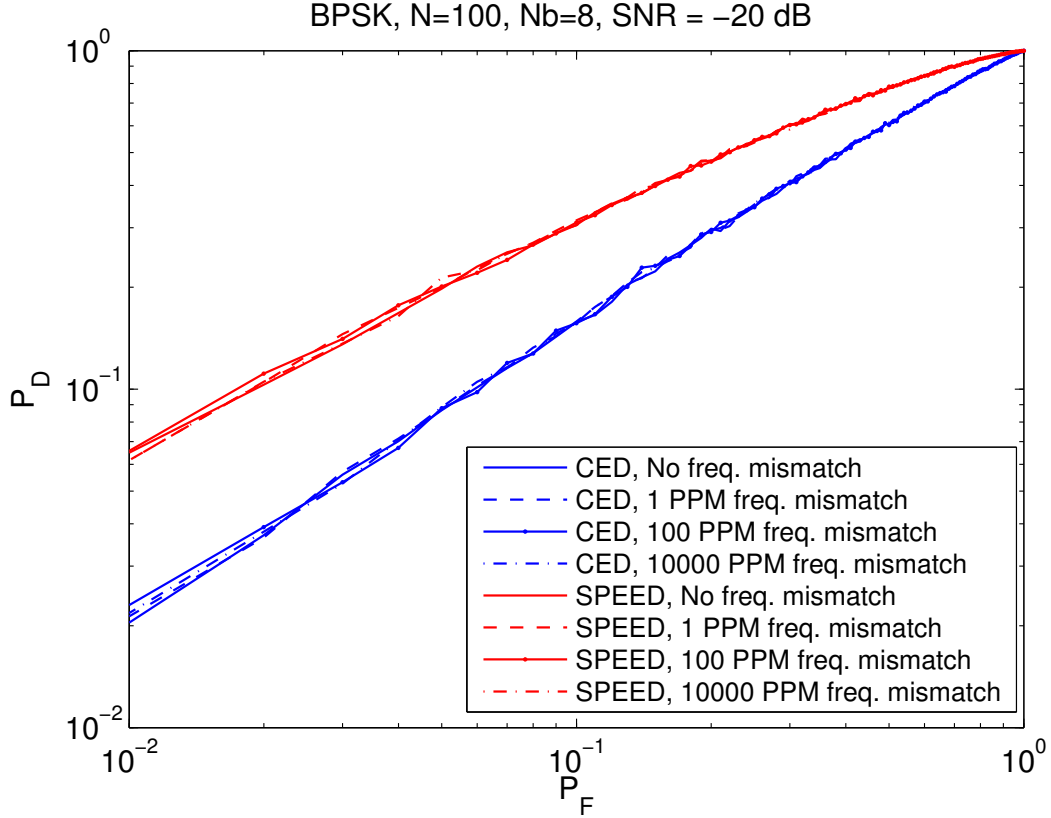
Figure 4.7: RoC for BPSK, $N = 100$, $N_b = 8$, SNR =-20 dB with 1, 100, 10000 PPM frequency mismatch in f_0 and f_s.

4.1.2 SNR Vs. P_D Simulations

We next present P_D for various SNR values ranging from -20 to 0 dB for a fixed $P_F = 0.01$ for all detectors. Figure 4.8 gives the plot for BPSK with $N = 100$ and $N_b = 8$ and Fig.4.9 gives the corresponding plot for BPSK with $N = 100$ and $N_b = 7$. Observe that IED is slightly better than CED at low SNR values but SPEED is better than all the detectors (and has a SNR gain of approximately 3 dB) at all the SNR values. We also give similar results for the case of 16-QAM in Fig.4.10 with $N = 100, N_b = 8$ and Fig.4.11, with $N = 100, N_b = 7$. From these plots, we can observe that SPEED performs much better than all other detectors at all SNR values for 16-QAM and BPSK signals. Note also that MSC performance is inferior to CED. This is because MSC estimation depends on correlation between the signal samples. When received signal is complex as in (3.5), MSC detector performance is inferior due to absence of spectral coherence as was shown in [12].
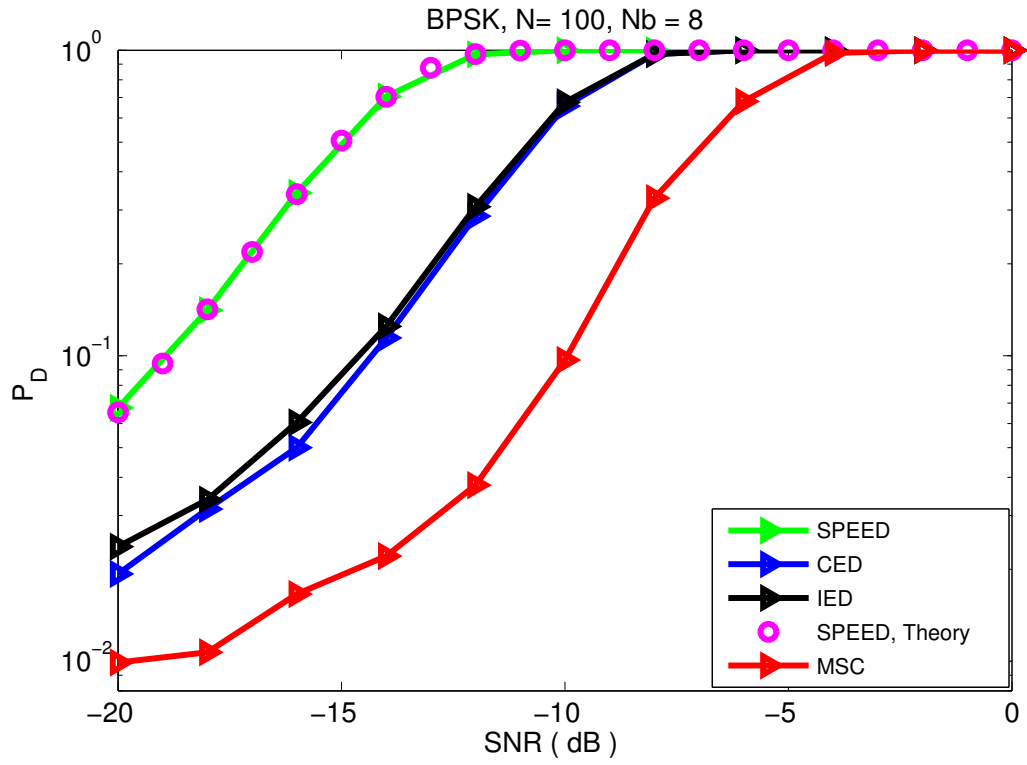
Figure 4.8: SNR vs. P_D for BPSK, $N = 100$, $N_b = 8$.
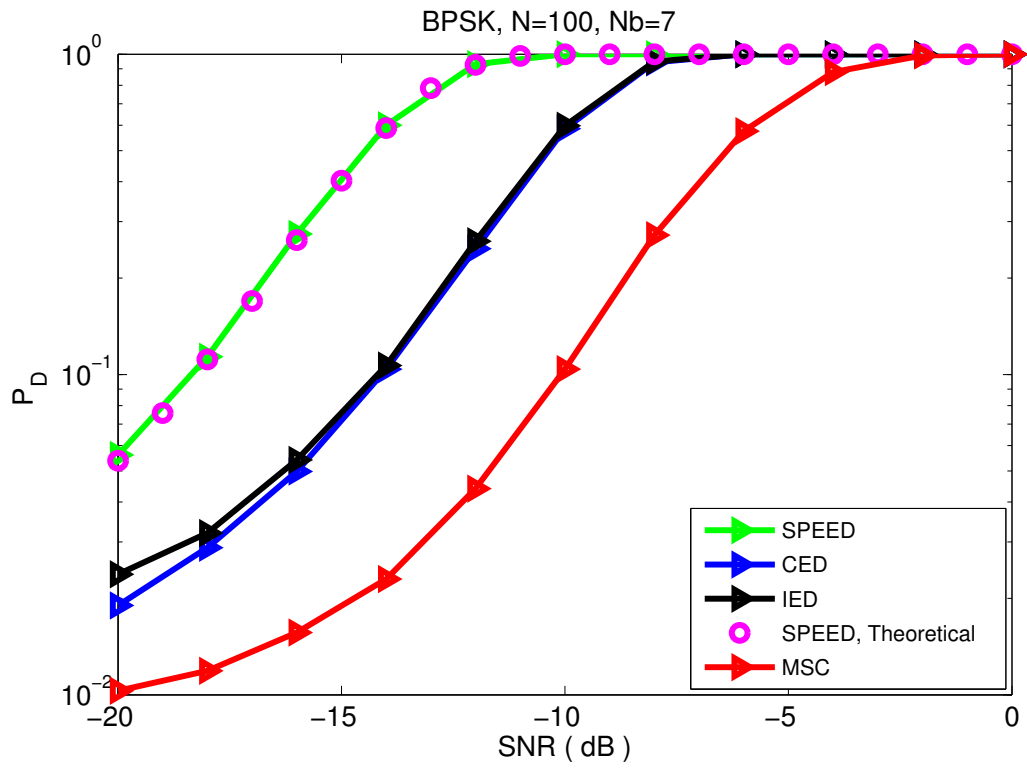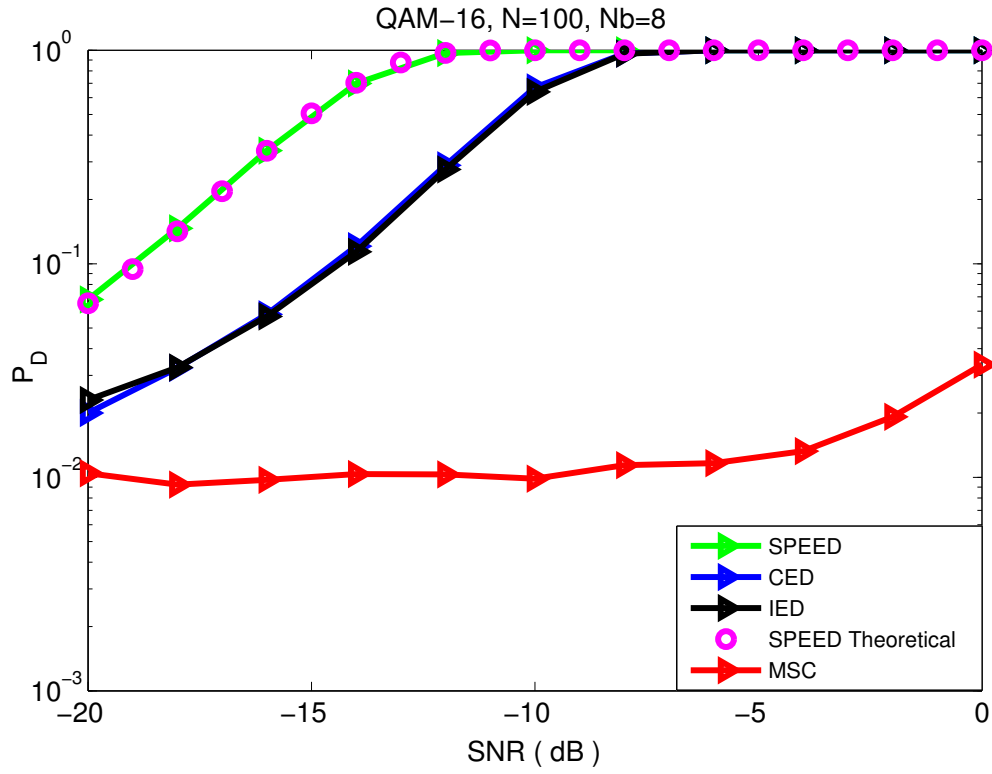
Figure 4.9: SNR vs. P_D for BPSK, $N = 100$, $N_b = 7$.

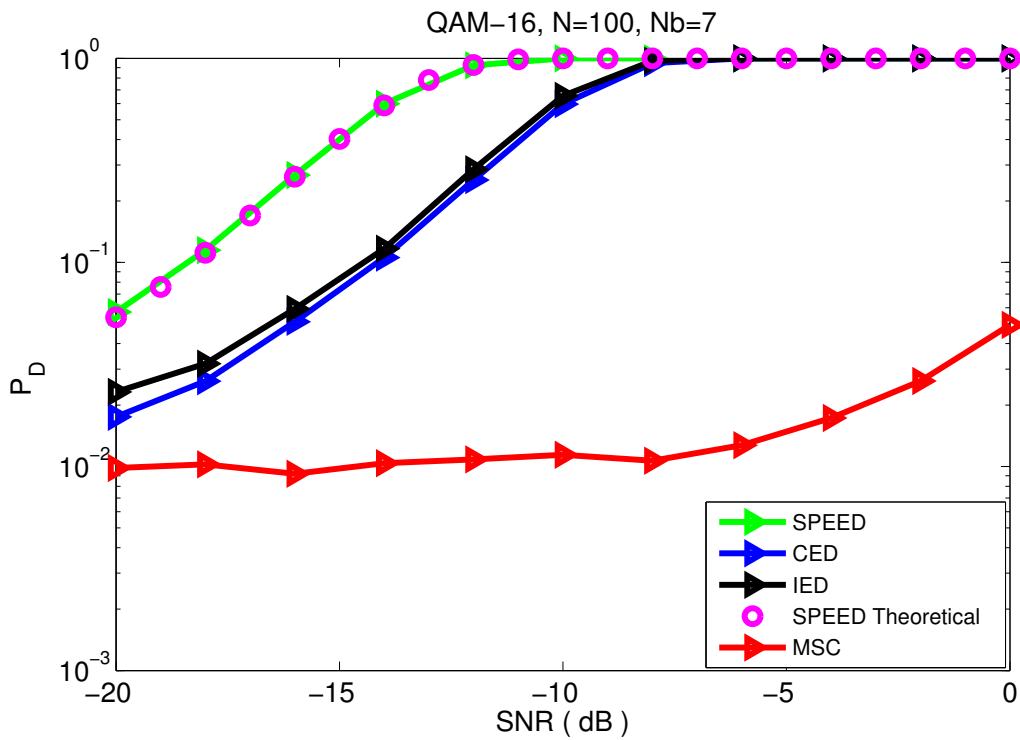Figure 4.10: SNR vs. P_D for 16-QAM, $N = 100$, $N_b = 8$.

Figure 4.11: SNR vs. P_D for 16-QAM, $N = 100$, $N_b = 7$.

4.2   Simulation results for $K > 1$

In these simulations, we take the carrier frequency of modulated waveform as $f_c = 1$ MHz, $f_0 = 500$ KHz and $K = 4$. We use [5], to simulate the performance of CED and IED. In IED, we use p values ranging from 1 to 10 with an interval of 0.1. For each P_F value, we choose a p value that maximizes the value of P_D. MSC detector is simulated using estimates as given in [2], and length of each segment(M) of the signal is considered as 64. CASE detector is simulated by using (3.12) for the case of N_k even and (3.11) for the case of N_k odd. We use (3.23), to give theoretical plots of CASE detector for N_k even and N_k odd cases. SNR values range from -20 to 0 dB are considered to plot SNR vs. P_D. In the first subsection, ROC plots of the detectors are given. SNR Vs. P_D plots are given in the second subsection of simulation results.

4.2.1   ROC Simulations

Fig.4.12 gives the simulation and theoretical results of ROC for CASE detector and CED in the case of 16-QAM signals with $N = 20$, $N_b = 24$ and $N_k = 6$ on left side of figure and with $N = 20$,$N_b = 20$ and $N_k = 5$ on right side of figure at SNR = -20 dB. From this plot, we can notice the exact match between theoretical and simulation results of CED and CASE detector. This plot clearly depicts the better performance of CASE detector than that of CED. We can also observe that as N_b increases, P_D of CASE detector is much better than that of CED. In Fig.4.13, we simulate the ROC plots of CED, IED, MSC detector and CASE detector in the case of BPSK signals with $N = 50$,$N_b = 24$ and $N_k = 6$ at SNR = -20 dB. This plot also shows the better performance of CASE detector than all other detectors. Since CASE detector has different teststatics for even and odd number of samples per perdiod (N_k), We give ROC plots of all detectors in the case of BPSK signals with $N = 50$, $N_b = 20$ and $N_k = 5$ at SNR = -20 dB in Fig.4.14. CASE detector also performs much better than all other detectors when N_k is odd for the case of BPSK signals.

Similarly, ROC of all the detectors are given for the case of 16-QAM signals with $N = 50$, $N_b = 24$ and $N_k = 6$ at SNR = -20 dB in Fig.4.15. With $N = 50$, $N_b = 20$ and $N_k = 5$ at SNR = -20 dB, ROC of all the detectors are given in Fig.4.16 for the case 16-QAM signals. From the given plots, we can notice that the observations given for BPSK signals also hold for 16-QAM signals.
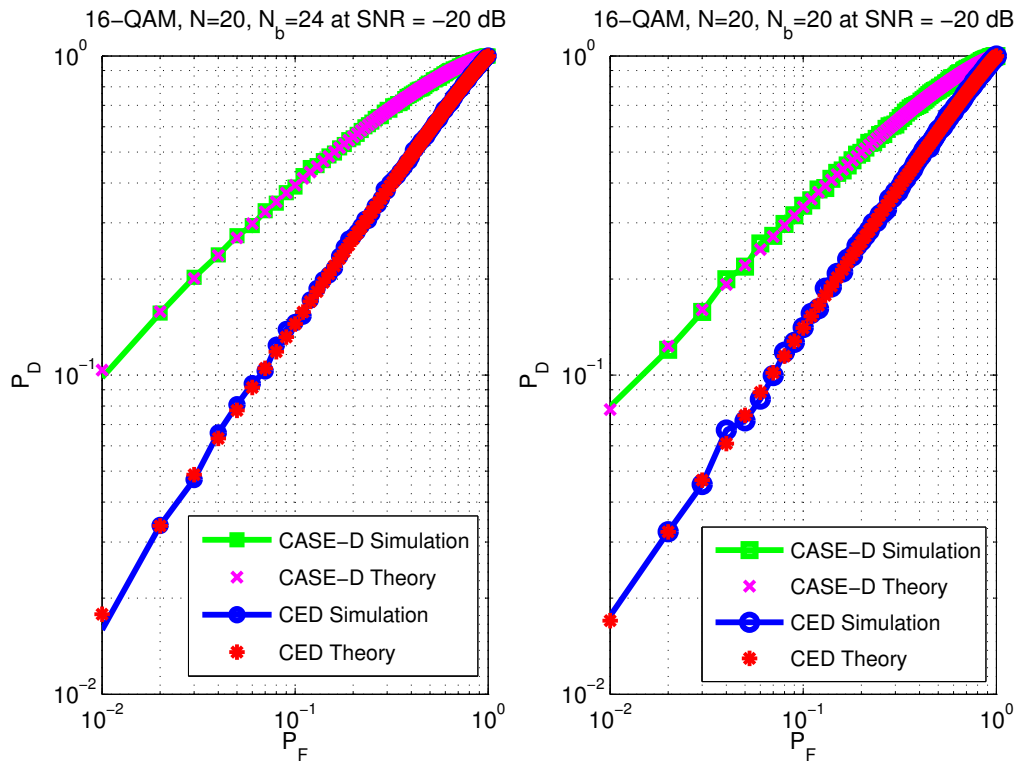
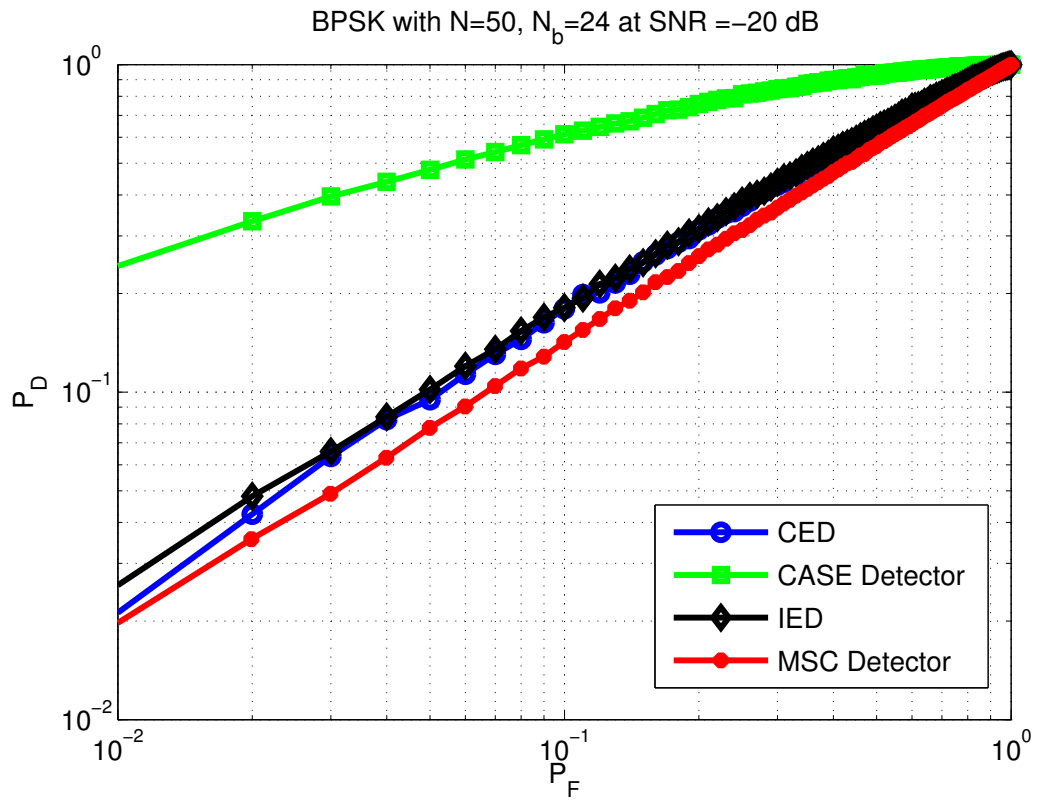Figure 4.12: ROC for 16-QAM with $N = 20$, $N_b = 24$ and 20.

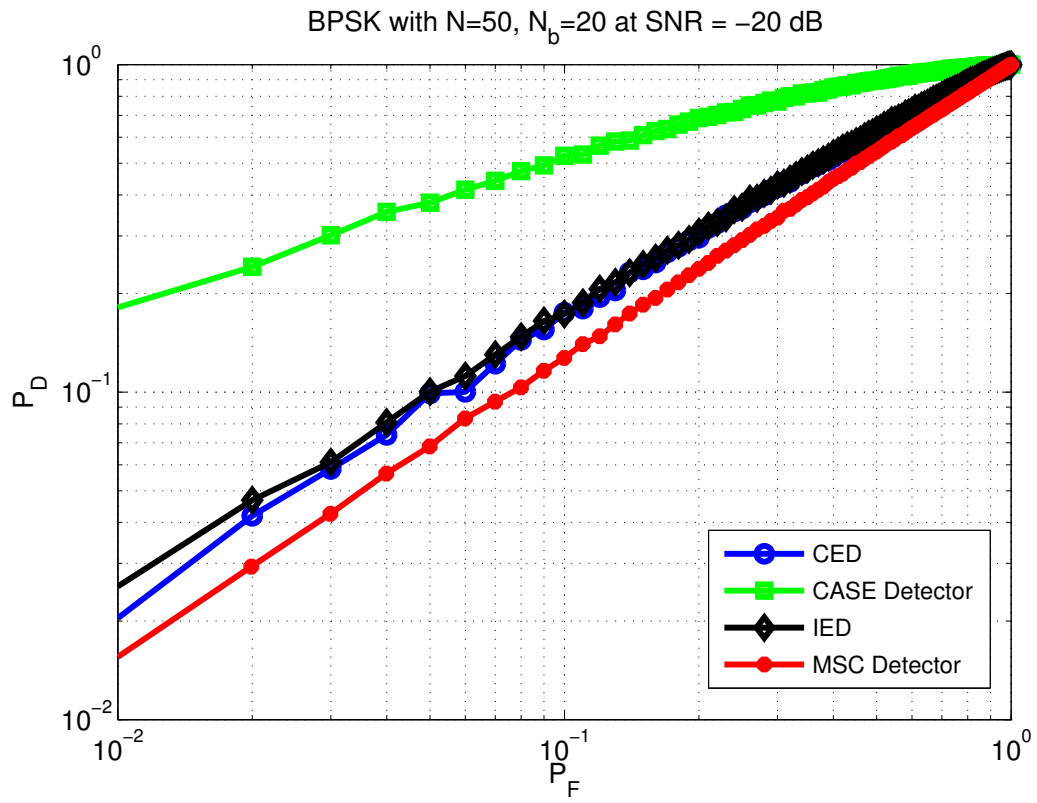Figure 4.13: ROC for BPSK with $N = 50$, N_b=24 and $N_K = 6$.

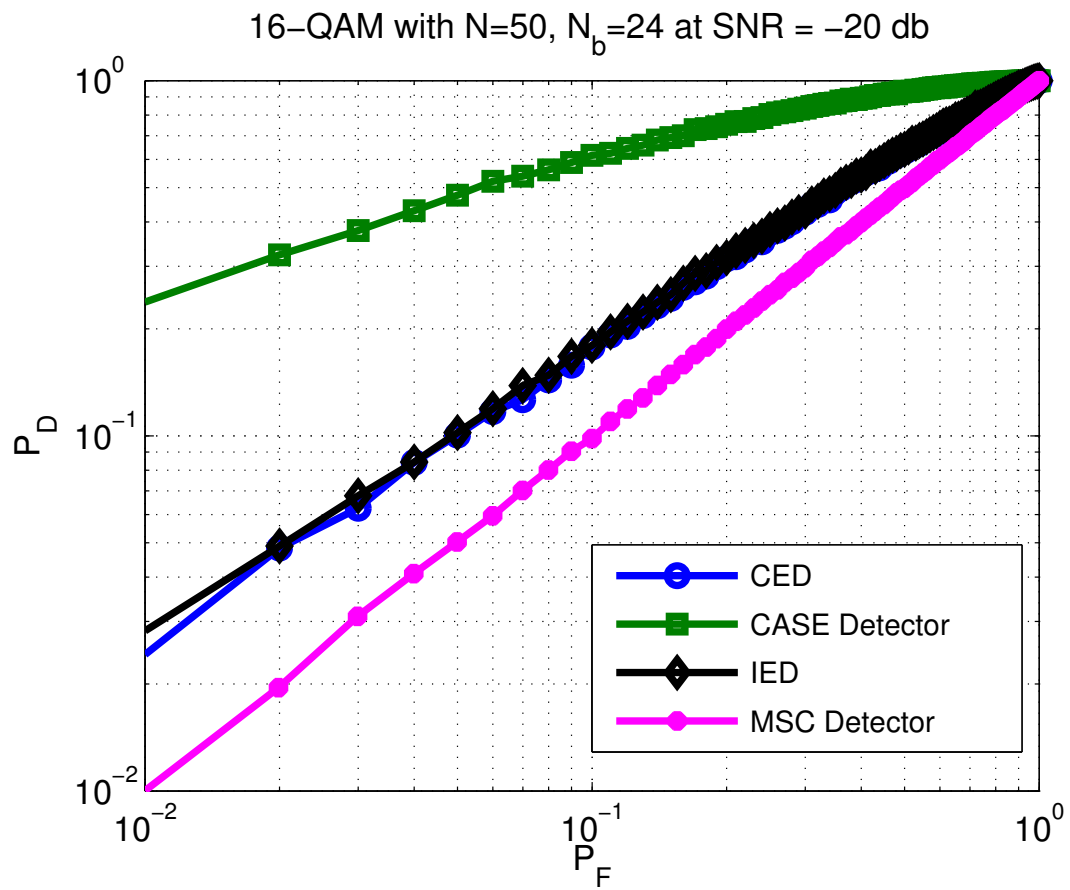Figure 4.14: ROC for BPSK with $N = 50$, $N_b = 20$ and $N_k = 5$.

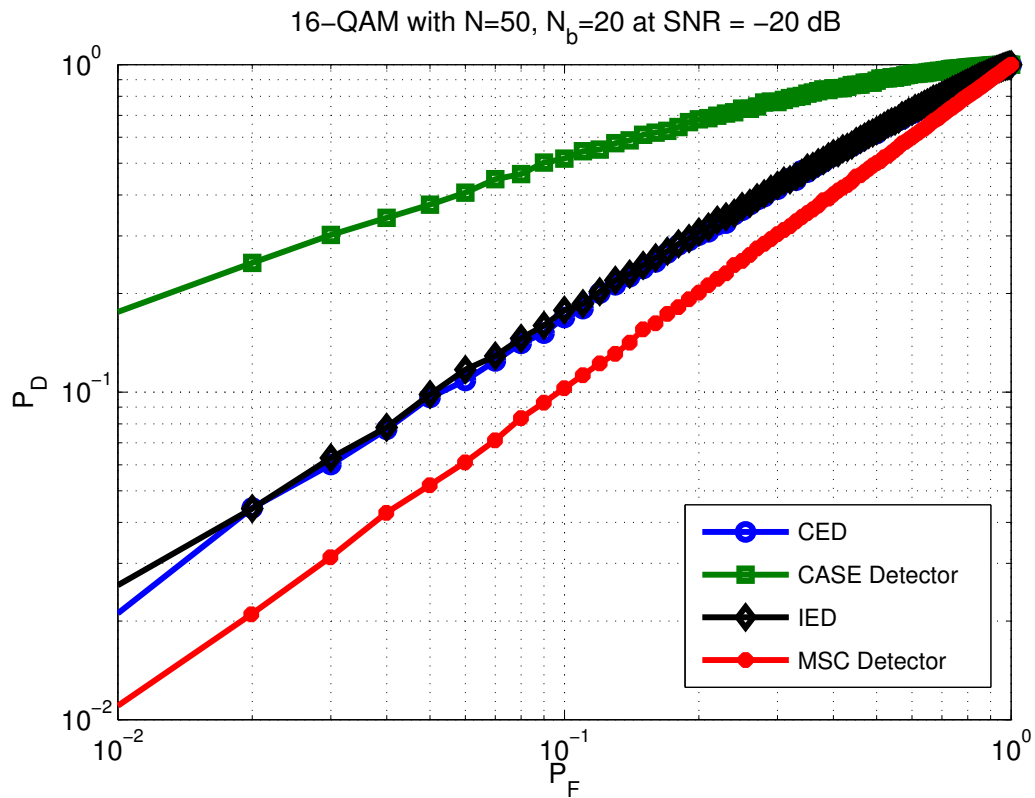Figure 4.15: ROC for 16-QAM with $N = 50$, $N_b = 24$ and $N_k = 6$.

Figure 4.16: ROC for 16-QAM with $N = 50$, $N_b = 20$ and $N_k = 5$.

We are interested to show the performance improvement of CASE detector as N_b increases. Hence, we give theoretical ROC plots of CASE detector and CED with $N = 20$, $N_b = 4, 8, 12, 16, 20$ and 24 at SNR = -20 dB. We can note that P_D of the CASE detector increases at the faster rate than that of CED. In practical situations, there is always some frequency mismatch at the receiver. Hence, we simulate the ROC of CASE detectors for 16-QAM signals with frequency mismatch of 1, 10 and 100 PPM in Fig.4.18 and show that CASE detector is as robust as CED for frequency mismatch.
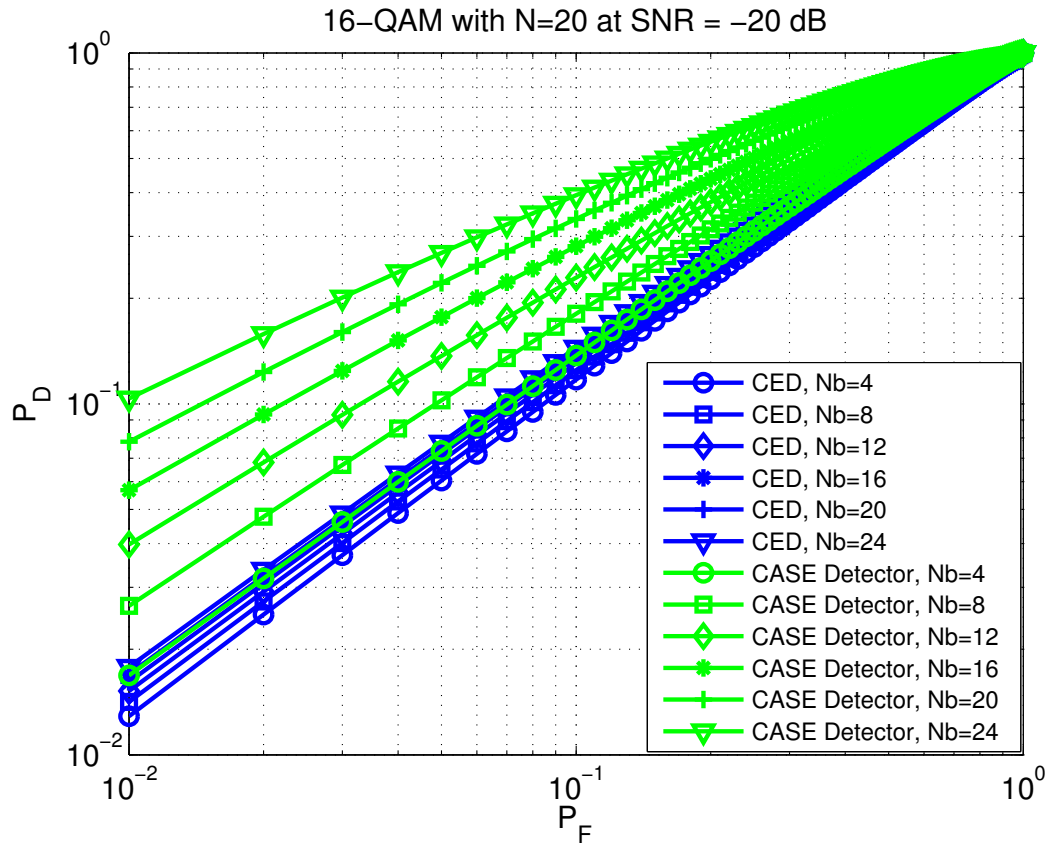
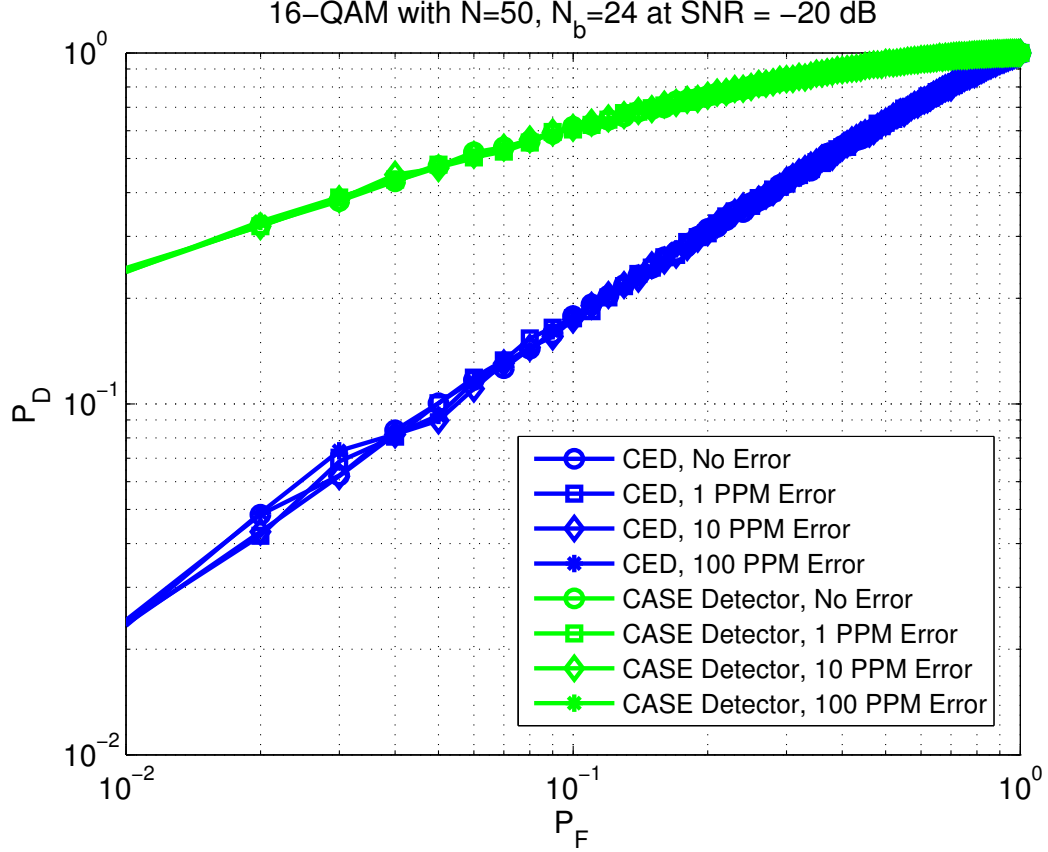Figure 4.17: ROC for 16-QAM with $N = 100$ and varying N_b at SNR = -20 dB.

Figure 4.18: ROC for 16-QAM with $N = 50$, $N_b = 24$ and $N_k = 6$ at SNR =-20 dB having frequency mismatch of 1, 10, 100 PPM in f_0 and f_s.

4.2.2 SNR Vs. P_D Simulations

To analyze further, we show the P_D for various SNR values ranging from -20 to 0 dB with a fixed $P_F = 0.01$ for all detectors. In Fig.4.19, we give the results for BPSK with $N = 50$, $N_b = 24$ and $N_k = 6$. In Fig.4.20, we give results for BPSK with $N = 50$, $N_b = 20$ and $N_k = 5$ to verify the performance of our detector when N_k is odd. We also give similar results for the case of 16-QAM in Fig.4.21 for $N = 50, N_b = 24$ and $N_k = 6$ and in Fig.4.22 for $N = 50, N_b = 20$ and $N_k = 5$. From these plots,we can observe that IED detector is slightly better than CED at low SNR values but CASE detector is always better than all other detectors and has more than 6 dB SNR gain for the given P_F and P_D values with $N_b = 24$ and $N_b = 20$. we can also notice that CASE detector performs much better than all other detectors at all SNR values for 16-QAM and BPSK signals. When received signal is of the form given in (3.5), MSC detector performance is very poor due to absense of spectral coherence as given in [12]. From the SNR vs. P_D plots of BPSK signals, we can observe that CED is always better than MSC detector at low SNR values. At high SNR values,

MSC detector is slightly better than CED when N_k is even and performance of MSC detector is comparable to that of CED when N_k is odd.
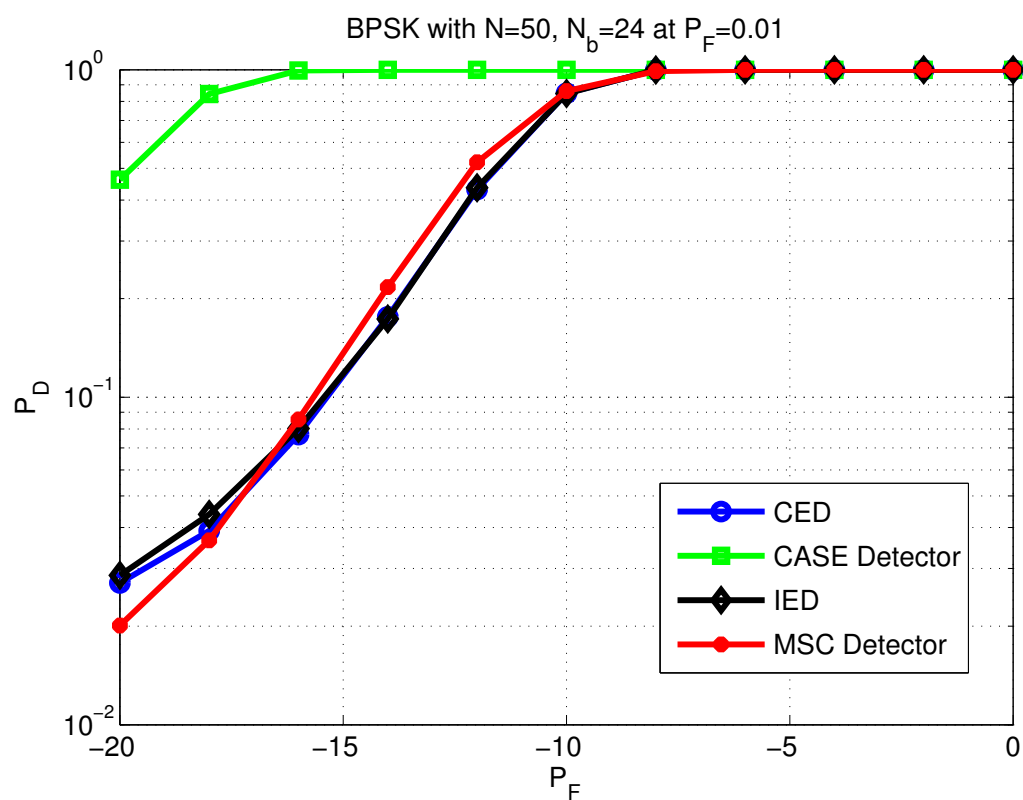

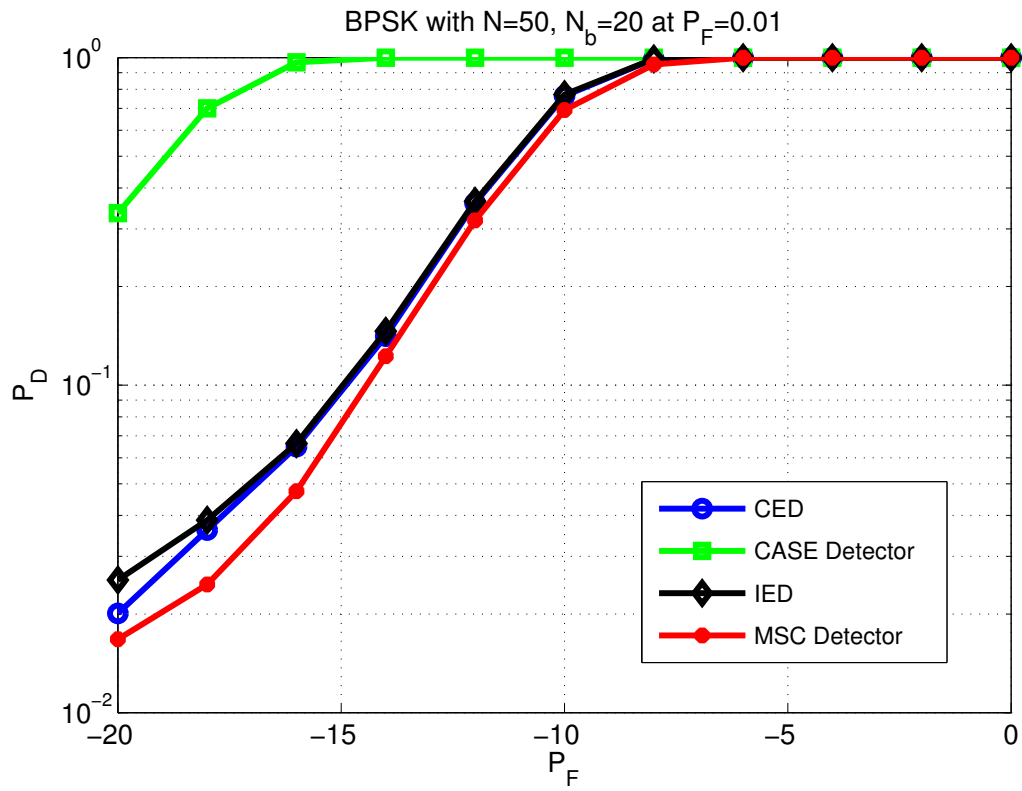Figure 4.19: SNR vs. P_D for BPSK with $N = 50$, $N_b = 24$ and $N_k = 6$.

Figure 4.20: SNR vs. P_D for BPSK with $N = 50$, $N_b = 20$ and $N_k = 5$.
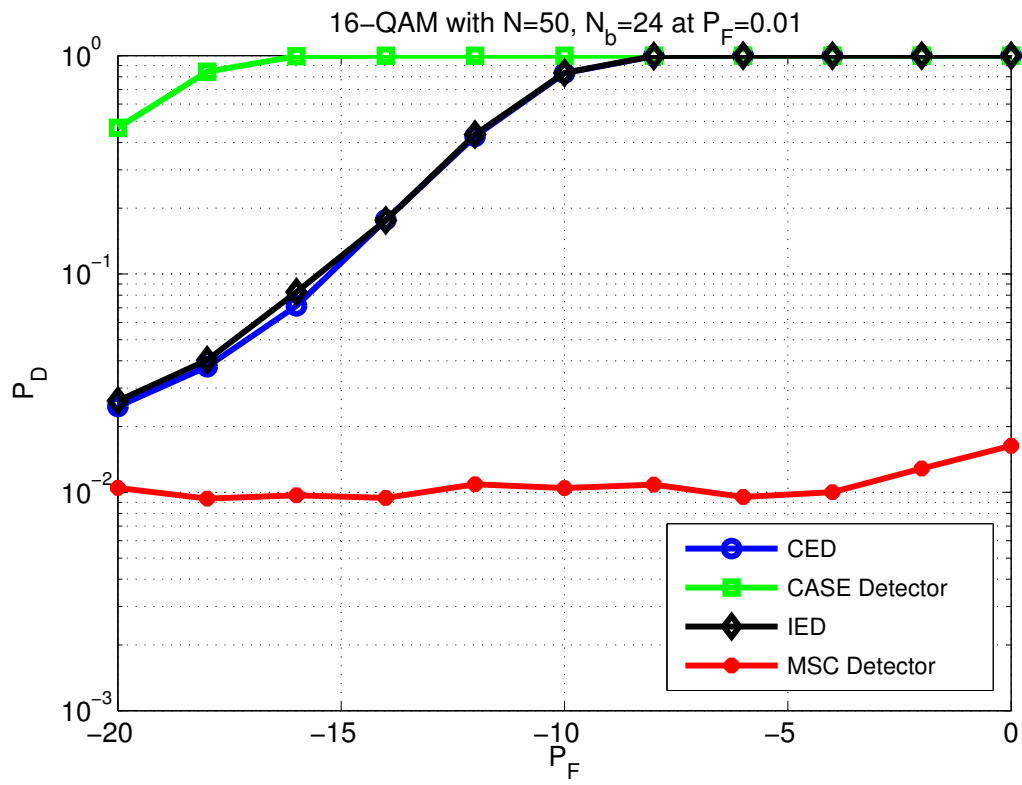
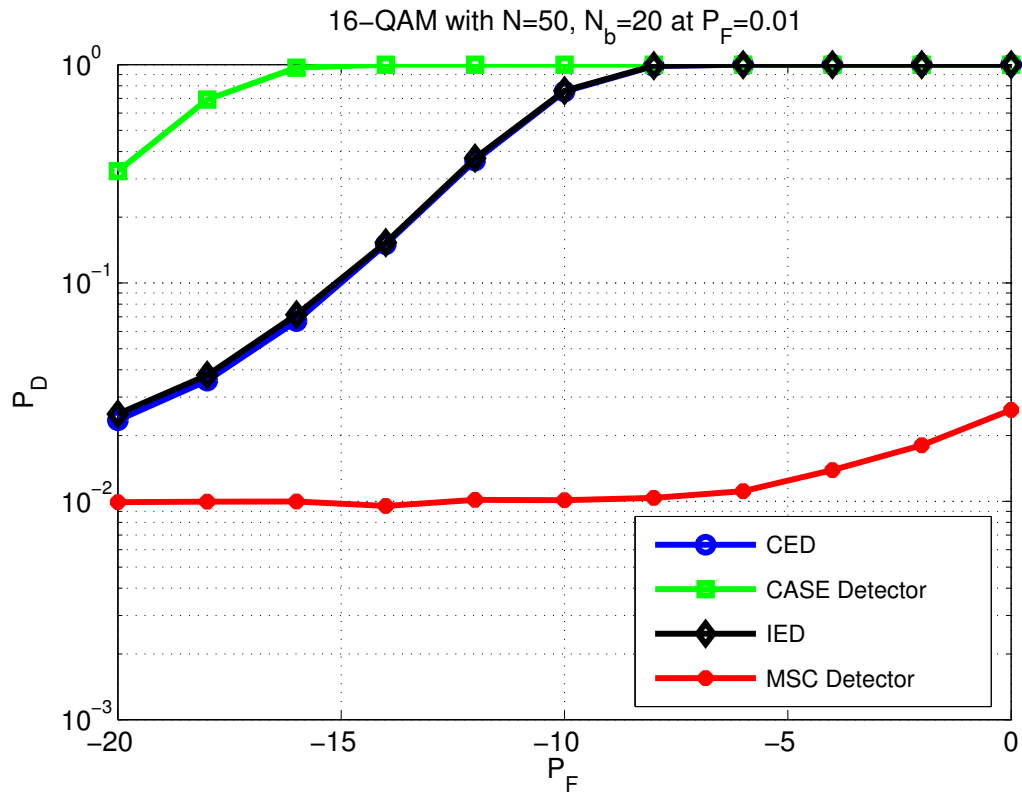Figure 4.21: SNR vs. P_D for 16-QAM with $N = 50$, $N_b = 24$ and $N_k = 6$

Figure 4.22: SNR vs. P_D for 16-QAM with $N = 50$, $N_b = 20$ and $N_k = 5$.

Chapter 5

Summary and Discussion

In this thesis, we give literature survey of three signal detection techniques named Conventional Energy Detector(CED), Improved Energy Detector(IED) and CycloStationary Detector(CSD). Detailed theoretical analysis of conventional energy detector along with simulation results are presented. Since Mathematical tractability of IED is very difficult, we give simulation results of IED in comparison with other detectors. As our target signal is digital modulation signals which possess some cyclostationary property, we give Magnitude squared detector(MSC) which is an example of cyclostaionary detector. As we can observe, IED is better than CED and CED is better than MSC. MSC performs better than CED when we have more number of signal samples and when the signal has good cyclic specral properties. MSC detector also depends on block size of FFT and it is computationally intensive.

As contribution of this thesis, we present a method for utilizing knowledge of symbol duration by appropriately selecting the sampling frequency and the intermediate frequency at the receiver. The proposed novel energy detector's performance depends on the knowledge of the signal period N_b, with computational complexity comparable to conventional energy detector. Exact analytical results along with simulations confirms the better performance of SPEED. As the number of samples per symbol duration increases the performance of the detector improves further. From the computational complexity analysis and simulation results, we can observe that SPEED with N_b even is superior to N_b odd. Since detection is a part of the receiver in almost all present wireless standards, wherein the symbol duration is known apriori, the proposed detector will be useful in detecting the signal. The proposed detector might also be useful in cognitive radio where it is essential to detect the signal in less time to improve spectrum utilization.

References

[1] T. Yucek and H. Arslan. A survey of spectrum sensing algorithms for cognitive radio applications. *IEEE Communications Surveys Tutorials* 11, (2009) 116–130.

[2] D. Bhargavi and C. R. Murthy. Performance comparison of energy, matched-filter and cyclostationarity-based spectrum sensing. In Signal Processing Advances in Wireless Communications (SPAWC), 2010 IEEE Eleventh International Workshop on. 2010 1–5.

[3] G. Staple and K. Werbach. The End of Spectrum Scarcity. *IEEE Spectr.* 41, (2004) 48–52.

[4] F. F. Digham, M. S. Alouini, and M. K. Simon. On the energy detection of unknown signals over fading channels. In Communications, 2003. ICC '03. IEEE International Conference on, volume 5. 2003 3575–3579 vol.5.

[5] Y. Chen. Improved energy detector for random signals in gaussian noise. *IEEE Transactions on Wireless Communications* 9, (2010) 558–563.

[6] R. S. Roberts, W. A. Brown, and H. H. Loomis. Computationally efficient algorithms for cyclic spectral analysis. *IEEE Signal Processing Magazine* 8, (1991) 38–49.

[7] W. Gardner. Measurement of spectral correlation. *IEEE Transactions on Acoustics, Speech, and Signal Processing* 34, (1986) 1111–1123.

[8] S. M. Kay. Fundamentals of Statistical Signal Processing: Estimation Theory. Prentice-Hall, Inc., Upper Saddle River, NJ, USA, 1993.

[9] M. Abramowitz and I. Stegun. Handbook of Mathematical Functions: With Formulas, Graphs, and Mathematical Tables. Applied mathematics series. Dover Publications, 1964.

[10] J. Proakis. Digital Communications. Electrical engineering series. McGraw-Hill, 2001.

[11] S. G. Johnson and M. Frigo. A Modified Split-Radix FFT With Fewer Arithmetic Operations. *IEEE Transactions on Signal Processing* 55, (2007) 111–119.

[12] A. Sahai, D. Cabric, N. Hoven, R. Tandra, M. Mishra, and B. Brodersen. Spectrum sensing: fundamental limits and practical challenges. Tutorial at Dyspan 2005 2005.